Modeling microbial diversity with metabolic trade-offs

Zhiyuan Li[1,2], Bo Liu[3], Sophia Hsin-Jung Li[4], Christopher G. King[5], Zemer Gitai[4], and Ned S. Wingreen*[4,6]

1. Center for the Physics of Biological Function, Princeton University.
2. Princeton Center for Theoretical Science, Princeton University.
3. Yuanpei College, Peking University, Beijing, China.
4. Department of Molecular Biology, Princeton University.
5. Department of Physics, Princeton University.
6. Lewis-Sigler Institute for Integrative Genomics, Princeton University, Princeton, NJ, USA

ABSTRACT

Nature exhibits much higher biodiversity than predicted by theories of competition. One solution for reconciling this "paradox of the plankton" is to imposes metabolic trade-offs, where species need to allocate limited cellular resources into multiple functions. However, two questions exist for metabolic models: first, as many such models have been proposed with diverse assumptions and different results, can we find a universal language to summarize various models into one unified framework? Second, under the pressure of evolution, will there be a single optimal metabolic strategy that finally dominates over all others? In this work, we address these two questions by constructing a generalizable framework to describe the species-environment feedback in chemostat-type resource-competition models. Employing this framework, a fitness landscape based on the strategy-growth rate relationship can be constructed. Species are capable of creating their own fitness landscape by shaping their nutrient environment, which allows for dynamic fitness landscapes and rich ecological behaviors, and is crucial for biodiversity in all the models we examined. A non-invasible strategy corresponds to a species creating a fitness landscape that places itself at the top. Under certain conditions, more than one species is required to complete this task, which leads to evolutionarily stable coexistence. Our approach facilitates quantitative understanding of chemostat experiments, and provides insight into the competitive-exclusion paradox.

INTRODUCTION

In the natural world, species are in constant competition. So why doesn't the fittest species outcompete the others and become the sole survivor? This question, captured by the "paradox of the plankton" (Hutchinson, 1961), has perplexed community ecologists for nearly a century. On the basis of simple resource-competition models, it has been argued that the number of stably coexisting species cannot exceed the number of resources, leading to the so-called competitive exclusion principle (Armstrong & McGehee, 1980; Hardin, 1960; Levin, 1970; McGehee & Armstrong, 1977). Nevertheless, tremendous biodiversity manifests in the real world, from environmental surveys to controlled lab experiments (Friedman, Higgins, & Gore, 2017; Goldford et al., 2018; Maharjan, Seeto, Notley-McRobb, & Ferenci, 2006). Even in well-mixed aquatic environments, hundreds of species of phytoplankton coexist on a few types of abiotic nutrients (Cermeño, Teixeira, Branco, Figueiras, & Marañón, 2014; Moore et al., 2013).

A multitude of hypotheses have been proposed to circumvent the competitive exclusion principle (Palmer, 1994; Roy & Chattopadhyay, 2007; Scheffer, Rinaldi, Huisman, & Weissing, 2003). Some introduce additional factors such as cooperative or antagonistic interactions between species (Bairey, Kelsic, & Kishony, 2016; Freilich et al., 2011; Kerr, Riley, Feldman, & Bohannan, 2002; Murdoch & Oaten, 1975; Venturelli et al., 2018; Wintermute & Silver, 2010), spatially structured habitats (Amarasekare, 2003; Geyrhofer & Brenner, 2018; Huisman, van Oostveen, & Weissing, 1999; D. Tilman, 1994), temporal fluctuations of the environment (Amarasekare, 2003; Behar, Brenner, & Louzoun, 2014; Descamps-Julien & Gonzalez, 2005; Huisman et al., 1999; D. Tilman, 1994), or complex life-histories of species (Huisman, Johansson, Folmer, & Weissing, 2001). Even in spatially homogeneous models with constant nutrient supply and without direct species interactions, rich dynamics have been uncovered under various conditions. In a model where species compete for essential resources, different nutrient requirements can produce intrinsically oscillatory or even chaotic dynamics that allows for increased diversity (Huisman & Weissing, 1999, 2001). Alternatively, cross-feeding (Goldford et al., 2018; Pfeiffer & Bonhoeffer, 2004), preferential nutrient utilization (A. Goyal, Dubinkina, & Maslov, 2018), or trade-offs (Beardmore, Gudelj, Lipson, & Hurst, 2011; Taillefumier, Posfai, Meir, & Wingreen, 2017) can promote stable coexistence. Recently, a simple model with a trade-off in nutrient uptake, was shown to self-organize to a state of unlimited coexistence (Posfai, Taillefumier, & Wingreen, 2017). This large variety of models and the richness of possible behaviors raises the question of unification: is there a simple framework that consolidates this diverse group of models into one easily understandable picture?

A key challenge to producing such a framework is that fitness landscapes are not static. Not only can extrinsic environmental factors fluctuate in space and time (Mustonen & Lässig, 2009), but species can also actively reshape their habitats (Laland, Matthews, & Feldman, 2016; Leibold, 1995; Odling-Smee, Laland, & Feldman, 2003). The feedback loop between species and their environment produces an intrinsically dynamic fitness landscape in which the action of one species can influence the fitness of all species. A

profound example is the Great Oxygenation Event, when cyanobacteria created an oxygen-rich atmosphere (Kasting & Siefert, 2002), causing a massive extinction of anaerobic bacteria but also stimulating an explosion of biodiversity (Schirrmeister, de Vos, Antonelli, & Bagheri, 2013). Today, species continue shaping their habitats on all scales: from humans inducing the sixth mass extinction (Ceballos et al., 2015) to microbes consuming nutrients, releasing wastes, and producing toxins (Callahan, Fukami, & Fisher, 2014).

Resource-competition models provide a simple context to explore the interaction between species and their environment (Smith & Waltman, 1995). In such models, species interact only indirectly, via consumption (and sometimes production) of a common pool of nutrients. A steady state can be reached if the species present can shape the nutrient concentration to support a growth rate equal to their dilution or death rate (David Tilman, 1982). Resource-competition models underpin many ecosystem theories including contemporary niche theory as pioneered by MacArthur (MacArthur, 1970), popularized by Tilman (David Tilman, 1980, 1982), and extended by Chase and Leibold (Chase & Leibold, 2003). A central component of contemporary niche theory is a graphical approach, generally consisting of three components: zero net growth isoclines (ZNGIs) in nutrient space, an impact vector representing a species' nutrient consumption, and a supply point to described the external resource supply (Koffel, Daufresne, Massol, & Klausmeier, 2016). This graphical approach is a powerful and intuitive way of evaluating the outcome of competition and community assembly, but has not been commonly utilized to understand models of coexistence (Letten, Ke, & Fukami, 2017), especially coexistence beyond the limit of competitive exclusion (Huisman & Weissing, 1999; Posfai et al., 2017).

In this work, we utilize and extend the graphical tools of resource-competition theory to relate and unify multiple models for microbial diversity, emphasizing the consequences of species creating their own environment. The nutrient environment shaped by one species through growth and consumption may be inviting or prohibiting to another species. We represent this species-environment interplay via an intuitive geometric visualization of a "rule of invasion". Under various model assumptions, the species-environment feedback allows intransitivity of fitness, in which there is no strict competition hierarchy and therefore no single best species or group of species (Soliveres et al., 2015). We demonstrate how such intransitivity can lead to rich ecosystem dynamics, including mutual invasion, multistability, and oscillations, and how all of these behaviors can be simply related via our graphical representation combined with the rule of invasion.

We extend our investigation of coexistence to encompass evolution. As species evolve to adapt to their environment, an ongoing threat to diversity is that mutation/selection may produce a supreme winner that takes over the habitat. To quantify the impact of evolution on biodiversity, we focus on models with metabolic trade-offs: with limited cellular resources, the growth rate of cells cannot increase without bound. Rather evolution optimizes over cells' internal resource allocation strategies (S. Goyal, Yuan, Chen, Rabinowitz, & Wingreen, 2010; Liebermeister et al., 2014). Different metabolic

strategies lead to different growth rates in different environments, driving a dynamic fitness landscape. From the perspective of species-environment feedback, we can define non-invasible/optimal metabolic strategies – namely, one or more species that construct a fitness landscape which places themselves on the top. When multiple species are indispensable in co-creating such an environment, their coexistence becomes evolutionarily stable.

RESULTS

Nutrient limitations, resource allocation strategies, and the chemostat

The growth of microbes is limited by the availability of external nutrients and by their own internal resources, including proteins and energy. Facing different stringencies, cells need to adjust the allocation of their limited internal resources toward a variety of cellular functions (nutrient import and assimilation, energy production, reproduction, maintenance, etc.) to achieve efficient growth. For example, in *E. coli* a large fraction of cellular resources is allocated to synthesize ribosomes, which is reflected in the RNA-to-Protein ratio (RP ratio). In a previous work, we used chemostats (Fig 1A) to quantitatively control growth rate and nutrient supply and showed that the RP ratio in *E. coli* is significantly lower under Phosphorus (P)-limitation than under Carbon (C)- or Nitrogen (N)-limitation at the same growth rates (Li et al., 2018), indicating cells adopt different proteome allocation strategies in response to different nutrient limitations. This observation raised further questions: How can we achieve fine control of nutrient limitation? Is the limiting nutrient determined by the absolute concentrations of supplied nutrients, or the relative abundance of one nutrient compared to the others?

To answer these questions, we ran chemostats at multiple growth rates and supply conditions, using RP ratio as a metric for P or C/N limitation. We started from a supply designed for P-limitation, i.e. with carbon and nitrogen supplied in excess, then kept the phosphate concentration in the supply unchanged but decreased the nitrogen concentration. If the nutrient limitation is controlled by the absolute concentration in the supply, cells should retain their RP ratio regardless of nitrogen supply. However, we observed that as the concentration of supplied nitrogen decreased, the RP ratios at all measured growth rates shifted up, from values reflecting P-limitation to values more characteristic of N-limitation, even though the supply of phosphorus remained at the initial “limiting” concentration (Fig 1B). Similar results were obtained for Carbon limitation (Fig 1C), where the RP-ratio curve was shifted to values resembling C-limitation over a series of dilutions of the carbon supply starting from P-limitation. These observed shifts of RP ratios indicate that nutrient limitation in a chemostat depends on the relative difference between supplied nutrients, rather than on the absolute concentration of any single supplied nutrient. Also, these observations highlight that non-intuitive behaviors can occur even in a system as simple as chemostat, highlighting the need for quantitative modeling.

The convergence towards steady state makes the chemostat an ideal experimental system to culture microorganisms and investigate their physiology with a constant environment and growth rate (Wides & Milo, 2018; Ziv, Brandt, & Gresham, 2013). Despite its simplicity, the chemostat captures an important property of ecosystems, namely that species create their own environment. For these reasons, many resource-competition models are based on chemostat-type dynamics. In the following sections, we present graphical representations that facilitate the interpretation of chemostat models and experiments, and provide intuitive understanding of a variety of resource-competition models via the lens of species-environment feedback.

A graphical representation of a chemostat model

In an idealized model of a chemostat (Fig 1A), p types of nutrients are supplied at rate d and concentrations $\vec{c}_{\text{supply}} = (c_{1,\text{supply}}, c_{2,\text{supply}}, \ldots c_{p,\text{supply}})$, meanwhile cells and medium are diluted at the same rate d. However, the environment that directly impacts cells is the nutrient concentration inside the chemostat, $\vec{c} = (c_1, c_2, \ldots c_p)$, which influences the intracellular metabolite concentrations $\vec{q}$ and the growth rate g of each species. Accordingly, the biomass density m of each species in the chemostat obeys:

$$\frac{dm}{dt} = m \cdot (g(\vec{c}, \vec{q}) - d). \quad (1)$$

The concentration c_i of the *i*-th nutrient is a variable, influenced by its rate of consumption by cells. For a single species with import rate I_i per cell volume, the concentration c_i satisfies

$$\frac{dc_i}{dt} = d \cdot (c_{i,\text{supply}} - c_i) - \frac{m}{r} \cdot I_i(\vec{c}, \vec{q}), \quad (2)$$

where *r* is a constant representing the biomass per cell volume. (If the volume of the chemostat is $V_{\text{chemostat}}$ and the total volume of cells is V_{cells}, the import flux of the *i*-th nutrient $V_{\text{cells}} \cdot I_i$ implies a rate of change of concentration inside cells of I_i and a corresponding rate of change of the concentration in the chemostat of $V_{\text{cells}} / V_{\text{chemostat}} \cdot I_i = (m \cdot V_{\text{chemostat}}/r)/V_{\text{chemostat}} \cdot I_i = m/r \cdot I_i$.)

In this manuscript, we define $\vec{c}$ as the "nutrient environment", and all possible values of $\vec{c}$ constitute the "nutrient space". Within a cell, the concentration of metabolites is influenced by intake rate, and influences the growth rate. Different metabolic models assume different forms for such influences, and we use $\vec{f}(\vec{I}(\vec{c}, q), \vec{q})$ to represent the rate of change of $\vec{q}$:

$$\frac{d\vec{q}}{dt} = \vec{f}(\vec{I}(\vec{c}, \vec{q}), \vec{q}). \quad (3)$$

Eqs. (1)-(3) represent a chemostat model in general. The simplicity of the chemostat has inspired many theoretical studies of resource competition, and different model assumptions about how species grow and consume nutrients have produced a variety of intriguing behaviors and conclusions. However, the origins of these differences are not always simple to discern. To provide a unified view, we present a graphical representation that allows ready visualization of the rich behaviors that emerge from the feedback between species and the environment in a chemostat.

We focus on steady-state behavior, where Eq. (3) is equal to zero and $\vec{q}$ can be solved for as a function of $\vec{c}$, reducing $g(\vec{c}, \vec{q})$ and $I_i(\vec{c}, \vec{q})$ to functions fully dependent on $\vec{c}$, namely $g(\vec{c})$ and $I_i(\vec{c})$. A graphical representation of the steady state created by a single species consists of three components (details in Methods):

1. *The growth contour* reflects how the nutrient environment determines cell growth. The growth-rate function $g(\vec{c})$ maps different points in nutrient space onto growth rates (background color in Fig 1D). At steady state, the relation $dm/dt = 0$ (Eq. (1)) requires the growth rate to be exactly equal to the dilution rate (assuming nonzero cell density). Therefore, the contour in nutrient space satisfying $g(\vec{c}) = d$ indicates all possible environments that could support the steady state of the species (red curve in Fig 1D).

2. *The flux-balance curve and the supply line* reflect how cells shape the nutrient environment for a given supply condition. At steady state, nutrient influx, dilution, and consumption need to be balanced such that $dc_i/dt = 0$ in Eq. (2). Flux balance can be expressed in two ways, depending on whether the unknown is the nutrient environment or the supply condition: First, given a supply condition, different values of cell density m lead to different steady-state nutrient concentrations (Eq. (S5)), constituting a one-dimensional "flux-balance curve" in nutrient space (purple, cyan, and blue curves in Fig 1D). Alternatively, given a specified steady-state nutrient concentration, different values of cell density m lead to a straight line in the space of supply conditions, which we call the "supply line" (see Methods for details). Despite the fact that the supply space and the nutrient space are distinct, they share the same units of concentration in each dimension. Therefore, for ease of visualize we typically show supply lines along with other features in the nutrient space (Eq. (S6), black dashed line in Fig 1D).

3. *The steady-state nutrient environment* $\vec{c}_{\mathrm{ss}}$ created by the species is the intersection of the growth contour and the flux-balance curve (Fig 1D, red dot). Due to consumption by the cells, $\vec{c}_{\mathrm{ss}}$ is less than $\vec{c}_{\mathrm{supply}}$ for all nutrients.

Subtleties in the control of nutrient limitation

The ability of cells to create their own nutrient environment brings complexity to chemostat experiments. In this section, we present two examples of subtleties in the control of nutrient limitation, and show how a graphical representation can assist in interpreting the experiments.

First, as all the $\vec{c}_{\mathrm{supply}}$ on one supply line correspond to a single steady-state $\vec{c}_{\mathrm{ss}}$, the resulting nutrient limitation in a chemostat depends on the difference between nutrient supplies, not on the absolute concentration of any single supplied nutrient. Different supply conditions (such as the purple, cyan, and blue open circles in Fig 1D), as long as they fall on the same supply line, can lead to identical steady-state nutrient environments (red dot in Fig 1D). Therefore, these supply conditions will lead to identical nutrient limitations and thus the same cellular response. This phenomenon is distinct from ratio-sensing, in which cells process dissimilar environmental inputs into similar responses (Escalante-Chong et al., 2015; Wang & Tang, 2017). The graphical result that the steady-state nutrient concentration and thus the nutrient limitation depends on the relative supply of different nutrients is consistent with our experimental observation (Fig 1B and C) that decreasing the nitrogen or carbon supply from a P-limited condition induces a similar proteome allocation as that induced by an N/C-limited supply with P in excess.

Interestingly, changing the dilution rate d alone has the potential to switch the limiting nutrient. As shown in Fig 1E, if the supply concentrations (blue open circle) are chosen to produce the blue flux-balance curve, this curve intersects with the yellow, orange, and deep red growth contours on the horizontal, horizontal, and vertical edges, respectively. Therefore, as the dilution rate and growth rate increase, the species will transition from nutrient *b*-limited to nutrient *a*-limited growth, even though the supply concentrations $\vec{c}_{\text{supply}}$ are kept unchanged.

Metabolic trade-off and strategies

As demonstrated by our R/P ratio measurements of *E. coli*, microorganisms allocate their limited internal resources according to the nutrient environment they perceive. In our models, We use α_j to denote the fraction of internal resources allocated to the j-th cellular function, with $\vec{\alpha} = (\alpha_1, \alpha_2 \ldots)$ representing a metabolic strategy. An exact metabolic trade-off is assumed, such that $\sum_j \alpha_j = 1$. For example, Figure 2A shows a simple metabolic model with two substitutable nutrients *a* and *b*, such as glucose and galactose (see Methods for details), that contribute linearly to biomass increase. Since a substantial investment of protein and energy is required for nutrient intake, the model assumes a trade-off between the allocation of internal resources to import either nutrient. Specifically, a fraction α_a of resources is allocated to import *a* and a fraction α_b (= $1 - \alpha_a$) to import *b.* All values of α_a from 0 to 1 define a continuous spectrum of metabolic strategies. How then shall we evaluate these strategies given that a single species adopting any one of these strategies will grow at exactly the same rate as dilution in a steady-state chemostat?

Rule of invasion

We use the outcome of competition between species to evaluate metabolic strategies, assuming each species adopts a given strategy. In particular, we focus on invasion: the introduction of a small number of an “invader” species to a steady-state chemostat already occupied by an “indigenous” species.

In the graphical representation of species-environment interaction, the outcome of an invasion can be summed up by a simple geometric rule, as demonstrated in Fig 2B and C. The growth contour of the invader (species *Red*) separate the nutrient space into two regions: an “invasion zone” where the invader grows faster than dilution (green-colored region in Fig 2B and C), and “no-invasion zone” where the invader has a growth rate lower than dilution. If the steady-state environment constructed by the indigenous species (species *Blue*) is located within the invasion zone of the invader, the invader will initially grow faster than dilution. Therefore, the invader will expand its population and the invasion will be successful (Fig 2B). By contrast, if the steady-state nutrient environment created by the indigenous species lies outside of the invasion zone, the invasion will be unsuccessful (Fig 2C, same species but different supply condition therefore different steady state). (See Methods for details.)

Mutual invasion, flat fitness landscape, and unlimited coexistence

Such a rule of invasion does not guarantee transitivity of competitiveness. That is, if species *Red* can invade species *Blue*, that does not mean *Blue* cannot invade *Red*.

Figure 2D shows an example of mutual invasibility. With a supply condition different from those in Fig 2B and C, while the steady-state environment created by *Blue* is located within the invasion zone of *Red*, the steady-state environment created by *Red* is also located within the invasion zone of *Blue*. According to the rule of invasion, each species can therefore invade the steady-state environment created by the other. In the face of such successful invasions, the only possible stable nutrient environment for this system is at the intersection of two growth contours, where the two species can coexist.

This mutual invasion can be readily understood within a "fitness-landscape" picture. Given an environment, we define the fitness landscape as the relation between the instantaneous growth rate and the metabolic strategy of any invader (Eq. (S8)-(S9), see Methods for details). Different environments give rise to different fitness landscapes. In the steady-state environment created by *Red* ($\alpha_a = 0.6$), strategies with smaller α_a have higher fitness (Fig 2D, upper inset, red curve). In the steady-state environment created by *Blue* ($\alpha_a = 0.2$), strategies with larger α_a have higher fitness (Fig 2D, upper inset, blue curve). Therefore, each species creates an environment that is more suitable for its competitor, which leads to coexistence.

For the environment co-created by *Blue* and *Red* (Fig 2D, purple dot), the fitness landscape becomes flat (Fig 2D, upper inset, purple curve): species with any metabolic strategy will grow at the same rate as dilution in this environment. Therefore, in this system, once a pair of species with a mutual-invasion relationship construct the nutrient environment together, all species become neutral and can coexist indefinitely (see Methods for details). This graphical approach to mutual invasion and the flat fitness landscape provide an intuitive representation of species self-organizing to a state of unlimited coexistence beyond competitive exclusion, as first reported by Posfai et al. (Posfai et al., 2017).

Rock-paper-scissor invasion loop and oscillation

Resource-competition models focusing on various aspects of cellular metabolism vary in their assumptions regarding $g(\vec{c},\vec{x},\vec{\alpha})$, $I(\vec{c},\vec{x},\vec{\alpha})$, and $f(\vec{c},\vec{x},\vec{\alpha})$, and can lead to diverse results for community structure and coexistence. However, the above general "rule of invasion" allows us to treat these divergent resource-competition models in a unified framework. In the following example, we utilized a metabolic model slightly different from that in Fig 2, to show that a dynamic fitness landscape is indispensable for coexistence.

In the metabolic model shown in Fig 3A, three substitutable nutrients, *a*, *b*, and *c*, contribute additively to cell growth. In this three-dimensional nutrient space, the growth contour for each species is a two-dimensional surface (Fig 3B). In addition to requiring enzymes to import the raw forms of these nutrients as in the model of Fig 2A, enzymes are also required to convert the imported raw materials into biomass. In this model, a six-element $\vec{\alpha}$ is required to describe the metabolic strategy, and there is the possibility of "mismatches" in the fraction of internal resources allocated to import and to convert the same nutrient. Such mismatches can produce a "rock-paper-scissor" invasion loop (Fig S1A): In the environment created by species 1, species 2 has a higher fitness but

not species 3; therefore species 2 can invade species 1 and establish its own environment; however, this environment lies within the invasion zone of species 3 (Fig 3B) but not of species 1, therefore species 3 subsequently invades; then in turn, species 3 create an environment where species 1 has the highest fitness. Such a loop of invasions leads to oscillatory population dynamics (Fig 3C, upper panel), with an ever-changing fitness landscape (Fig 3C, lower panel).

Oscillation and even chaos in resource-competition model have been demonstrated by Huisman et al. (Huisman et al., 1999), and shown to allow dynamical coexistence beyond competitive exclusion. The simple model presented here illustrates how oscillation can be understood as a loop of invasion creating an ever-changing fitness landscape.

Multi-stability, chain of invasion, and non-invasible strategies

When species create environments that are more favorable for their competitors, mutual-invasion and oscillations can occur. Can species create environments that are hostile to their competitors, and if so what will be the consequences?

Fig 4A shows a simple metabolic model with two essential nutrients *a* and *b*, such as nitrogen and phosphorus (see Methods for details). Similar to the model in Fig 2A, the model assumes a trade-off between the allocation of internal resources to import nutrients, so that a resource allocation strategy is fully characterized by the fraction of resources α_a allocated to import nutrient *a*. The growth rate is taken to be the minimum of the two input rates (Odum & Barrett, 1971). As shown in Fig 4B, two species, *Red* and *Blue*, each creates a nutrient environment outside of the invasion zone of each other. According to the rule of invasion, neither can be invaded by the other. Therefore, the steady state of the community depends on initial conditions – whichever species occupies the chemostat first will dominate indefinitely.

From the perspective of the strategy-growth relationship (Fig 4B, inset), species *Red* ($\alpha_a = 0.65$) creates a fitness landscape where small α_a is disfavored. Symmetrically, species *Blue* ($\alpha_a = 0.35$) creates a fitness landscape where large α_a is disfavored. However, neither *Red* nor *Blue* sits on the top of the fitness landscape each one creates (Fig 4C). In the fitness landscape created by *Blue*, a slightly larger α_a (green diamond in Fig 4C) has the highest growth rate. Consequently, species adopting the *Green* strategy can invade *Blue*. Nevertheless, species *Green* is not on the top of its own fitness landscape as an even larger α_a (yellow diamond in Fig 4C) maximizes the growth rate in the environment created by *Green*. A series of replacements by the fastest-growing species in the environment created by the former species creates a chain of invasion.

It is worth noting that in this model after four steps of replacement, bistability appears. The species with α_a marked by *Deep Purple*, which is reached by the chain of invasion going from *Blue*, to *Green*, to *Yellow*, to *Deep Green*, cannot invade the original species *Blue*. A similar relationship holds between *Cyan* and *Red*. This phenomenon highlights the difference between ecological stability and evolutionary stability: Ecologically, as both *Blue* and *Deep Purple* create a fitness landscape where the other species grows slower than dilution, they constitute a bistable system. However, evolutionarily, mutants

with slightly larger α_a can invade *Blue,* bringing the system towards *Deep Purple* until bistability collapses.

In this model, with symmetric parameters, the only evolutionarily stable strategy is $\alpha_a = 0.5$ (black diamond in Fig 4C). This is the only strategy that locates itself on the top of the fitness landscape it creates, and therefore cannot be invaded by any other species. This simple model demonstrates a general definition of evolutionarily stable (aka optimal or non-invasible) strategies: those strategies that create a fitness landscape which places themselves on the top (Eq. (S10)).

A nutrient environment defines a fitness landscape, and the steady-state nutrient environment created by species is influenced by supply condition, dilution rate, and cell metabolism. Therefore, different chemostat parameters and different metabolic models lead to different optimal strategies. In the following, we described a generally applicable protocol for obtaining the non-invasible strategies, using the metabolic model in Fig 4A as the example (Fig 4D, details in Methods):
First, under a nutrient environment $\vec{c}$, the maximal growth rate $g_{\max}(\vec{c})$ (background color in Fig 4D) and the corresponding resource allocation strategy $\vec{\alpha}_{\max}(\vec{c})$ can be obtained analytically or via numerical search through the strategy space (Eq. (S11)). $g_{\max}(\vec{c})$ and $\vec{\alpha}_{\max}(\vec{c})$ are independent of the chemostat parameters $\vec{c}_{\text{supply}}$ and d.
Second, the maximal growth contour for dilution rate d is defined as all nutrient environments $\vec{c}$ that support a maximal growth rate of d (Eq. (S12)). Different maximizing strategies $\vec{\alpha}_{\max}(\vec{c})$ exist at different points of the maximal growth contour, as shown by the colors of the curve in Fig 4D. By definition, the maximal growth contour envelops the growth contour of any single strategy, and nutrient environments on the maximal growth contour are outside of the invasion zone of any strategy. Therefore, if a species is able to create a steady-state environment on the maximal growth contour, it cannot be invaded. Finally, different $\vec{c}_{\text{supply}}$ form different maximal flux-balance curves (Eq. (S14)), which intersect with the maximal growth contour at one point $\vec{c}_{\text{opt}}$. Species $\vec{\alpha}_{\max}(\vec{c}_{\text{opt}})$ that adopt the maximizing strategy at $\vec{c}_{\text{opt}}$ create the environment $\vec{c}_{\text{opt}}$, and are therefore immune to invasion. Under different $\vec{c}_{\text{supply}}$, different species become non-invasible (orange, green, and blue growth contours in Fig 4D), and the supply lines emanating from different points on the maximal growth contour indicate the supply conditions for which the corresponding strategies are evolutionarily stable.

Evolutionarily stable coexistence

Given d and $\vec{c}_{\text{supply}}$, the maximal growth contour and the maximal flux-balance curve are unique, therefore there is only one $\vec{c}_{\text{opt}}$. Does the uniqueness of $\vec{c}_{\text{opt}}$ imply a single evolutionarily stable species? Or is coexistence still possible even in the face of evolution? In a recent work (Taillefumier et al., 2017), this question was addressed by modeling a population of microbes competing for steadily supplied resources. Though *in-silico* evolution and network analysis, the authors found that multiple species with distinct metabolic strategies can coexist as evolutionarily-stable co-optimal consortia, which no other species can invade.

Using a simplified version of Taillefumier et al.'s model (Fig 5A), we employ the graphical approach to help identify the requirements for such evolutionarily-stable coexistence and the role of each species in supporting the consortium. In this model, at the cost of producing the necessary enzymes, cells are not only able to import external nutrients, but can also convert any one of the internal nutrients into any other. Meanwhile, nutrients passively diffuse in and out of the cell. The internal concentrations of nutrient *a* and nutrient *b* are both essential for cell growth (see Methods for detail). Therefore, metabolic trade-offs in this system have four elements: the fraction of internal resources allocated to import nutrient *a* (α_a) or nutrient *b* (α_b) and/or convert one nutrient into another (α_{ab} converts internal *b* into *a,* and α_{ba} converts internal *a* into *b*). Each species is defined by its internal resource allocation strategy $\vec{\alpha} = (\alpha_a, \alpha_b, \alpha_{ab}, \alpha_{ba})$.

Following the general protocol described in the previous section, we first identified the maximal growth rates $g_{\max}(\vec{c})$ and the corresponding strategy or strategies $\vec{\alpha}_{\max}(\vec{c})$ at each point $\vec{c}$ in the nutrient space, and generated maximal growth contours for different dilution rates (Fig 5B). The maximal growth contours are not smoothly continuous, nor are the corresponding strategies. In nutrient space, three distinct sectors of maximizing strategies appear (Fig 5B, Fig S3A): When nutrient *a* is very low compared to *b*, the maximizing strategy is a "*b*-*a* converter" which imports *b* and converts it into *a* (blue sector, only α_b and α_{ab} are non-zero). Symmetrically, when *a* is comparatively high, the optimal strategy is a "*a*-*b* converter" (green sector, only α_a and α_{ba} are non-zero). Otherwise, the maximizing strategy is an "importer" which imports both nutrients without conversion (red sector, only α_a and α_b are non-zero). On the border between sectors, the maximal growth contour has a discontinuous slope.

Evolutionarily stable coexistence occurs at these discontinuous points. If an environment point $\vec{c}_0$ is located in a continuous region of the maximal growth contour, only one maximizing strategy $\vec{\alpha}_{\max}(\vec{c}_0)$ exists for that environment (maximizing strategies along the maximal growth contour are indicated by colored squares in Fig 5C). Supply conditions that make $\vec{\alpha}_{\max}(\vec{c}_0)$ the optimal strategy (i.e. allow $\vec{\alpha}_{\max}(\vec{c}_0)$ to create the steady-state environment $\vec{c}_0$) constitute the supply line for $\vec{c}_0$ and $\vec{\alpha}_{\max}(\vec{c}_0)$. However, at the discontinuous points of the maximal growth contour, where two classes of strategies meet, two different strategies are both maximizing. For example, at the purple dot in Fig 5C a strategy belonging to the "*b*-*a* converter" class (species *Blue*) and one belonging to the "importer" class (species *Red*) are both maximizing strategies. Each strategy derives a supply line from the purple dot (black dashed line, Fig 5C). The two supply lines span a gray region where no supply line from any single strategy enters. Correspondingly, for any supply conditions inside the gray region, no single species can alone create an environment on the maximal growth contour. For example, under the supply condition shown by the black open circle in the gray region, species *Blue* and species *Red* both create nutrient environments that lie within the maximal growth contour (blue and red dots, Fig 5C), and are thus subject to invasion by other species. Nevertheless, the species-specific growth contours of *Blue* and of *Red* intersect at the purple point on the maximal growth contour. Therefore, only when *Blue* and *Red* coexist can they co-create an environment on the maximal growth contour, and thus resistant to invasion from any other species. Indeed, when we simulate

multiple species with different maximizing strategies under the supply condition indicated by the open black circle, species *Blue* and species *Red* are the only two that survive (Fig 5C, inset).

The optimal coexistence of species *Blue* and species *Red* can be understood intuitively from the dynamic fitness landscape. Given a nutrient environment, the relation between α_a and growth rate of importer (red curve) or *a*-*b* converter (green curve), and that between α_b and growth rate of *b*-*a* converter (green curve) constitute the fitness landscape of species adopting different possible maximizing strategies (Fig 5D). In the environment created by species *Blue* (blue dot in Fig 5C), not only will some importers grow faster than *Blue*, species *Blue* (strategy marked by blue diamond) is not even on the fitness peak of its own class (Fig 5D, upper box). Similarly, in the environment created by species *Red*, the strategy of *Red* is not at the top of the fitness landscape (Fig 5D, middle box). By contrast, in the environment co-created by species *Blue* and *Red* (purple dot in Fig 5C), their strategies are at the top of the fitness landscapes of their own classes and at equal height. For all supply conditions in the gray region, species *Blue* and species *Red* jointly drive the nutrient concentrations to the discontinuous point of the optimal growth contour, and thereby achieve evolutionarily stable coexistence.

Species creating a new nutrient dimension

As discussed in the introduction, one possible solution to the paradox of plankton is the creation of new nutrient "dimensions" by species secreting metabolites that can be utilized by other species. For example, *E. coli* secretes acetate as a by-product of glucose metabolism. Accumulation of acetate impedes the growth of *E. coli* on glucose (Luli & Strohl, 1990), but the acetate can be utilized as a carbon source by mutant strains that emerge in long-term evolution experiments (D'Souza et al., 2018; Rosenzweig, Sharp, Treves, & Adams, 1994).

To explore the possibilities of evolutionarily stable coexistence when species create new nutrients, we used a simplified model to represent multi-step energy generation with a dual-role intermediate metabolite (Fig 6A). A single chemical energy source S is supplied into the chemostat. The pathway for processing S consists of four relevant reactions driven by designated enzymes: External S can be imported and converted into intermediate I_{int} to generate ATP (with corresponding fraction of enzyme budget α_{ATP1}).The intermediate has a dual role in energy production: on the one hand, it positively contributes to ATP production via a downstream reaction (with fraction of enzyme budget α_{ATP2}); on the other hand, it negatively contributes to ATP production through product inhibition of the first energy-producing reaction. To deal with the negative effect of internal intermediate, cells may synthesize transporters to export intermediate out into environment, where it becomes external intermediate I_{ext} (fraction of enzyme budget α_{exp}). By this reaction, cell can increase the dimension of nutrient space from one (S) into two (S and I_{ext}). Cells can also import I_{ext} into I_{int} (fraction of enzyme budget α_{imp}), then use I_{int} as an energy source via the second reaction. (See Methods for details.)

The metabolic strategy $\vec{\alpha}$ in this model has four components: $\vec{\alpha} = (\alpha_{\mathrm{ATP1}}, \alpha_{\mathrm{ATP2}}, \alpha_{\mathrm{exp}}, \alpha_{\mathrm{imp}})$. When we examine the maximizing strategies and maximal growth rates in the nutrient space, three distinctive classes of strategy emerge (Fig 6B). When S is abundant and I_{ext} is low, the maximizing strategies have only two non-zero components, α_{ATP1} and α_{exp} (Fig S3B), meaning this class of species only imports S for the first energy-generating reaction then exports intermediate as waste. Therefore, we call strategies in this class "polluters" (blue section in Fig 6B, Fig S3C). When I_{ext} is high while S is low, the maximizing strategies have two different non-zero components, α_{ATP2} and α_{imp} (Fig S3B), meaning this class of species solely relies on I_{ext} as its energy source. We call these strategies "cleaners" as they clean up the I_{ext} in the environment, which is detrimental to the polluters (green section in Fig 6B, Fig S3C). When there are comparable amounts of S and I_{ext} present, a third class of maximizing strategies appears: these cells neither export nor import intermediates, but rather allocate all enzyme budget to α_{ATP1} and α_{ATP2} to carry out both energy-producing reactions. We call species in this class "generalists" (red section in Fig 6B, Fig S3C).

As shown in Fig 6B, on the borders between classes of strategies in nutrient space, the maximal growth contours turn discontinuously. These points of discontinuity, as in the previous section, are nutrient environments corresponding to evolutionarily stable coexistence of species from distinct metabolic classes. The classes of optimally coexisting species change with dilution rate. When the dilution rate is low ($d = 0.4$, Fig 6C), at the discontinuous point of the maximal growth contour, the corresponding two maximizing strategies are one polluter (species *Blue*) and one cleaner (species *Green*). Their supply lines span a gray region where both species *Blue* and species *Green* are required to create a steady-state environment on the maximal growth contour. As we are only supplying the system with S, the supply condition always lies on the *x*-axis of concentration space. For the supply condition shown by the black open circle in Fig 6C, polluter *Blue* creates a nutrient environment (blue dot) far from the maximal growth contour. When the cleaner *Green* is added to the system, not only does the biomass of *Blue* increase (inset), but also the steady-state nutrient environment moves to the discontinuous point of the maximal growth contour (cyan dot), where both *Blue* and *Green* occupies the peaks of their fitness landscapes (Fig 6D). This result is consistent with the long-term evolution experiment of *E. coli* and also intuitive: polluter *Blue* and cleaner *Green* form a mutually beneficial relationship by, respectively, providing nutrients and cleaning up waste for each other, thereby reaching an optimal cooperative coexistence.

A quite different coexistence occurs at higher dilution rate ($d = 0.6$, Fig 6E). Growth contours at this dilution rate show two turning points, but neither are between the polluter and the cleaner class. One discontinuous point is between the cleaner class (green squares) and the generalist class (red squares), but the gray region spanned by the corresponding supply lines does not cover the *x*-axis and so does not represent an attainable coexistence when only S is supplied. The other discontinuous point is between the generalist class and the polluter class (blue squares). The gray region spanned by the supply lines of the corresponding two maximizing strategies of generalist class (species *Red*) and polluter class (species *Blue*) does cover the *x*-axis.

Therefore, a supply condition with only S within the gray region (e.g., the black open circle) leads to the optimal coexistence of generalist *Red* and polluter *Blue* on the discontinuous point (purple dot), despite the fact that they do not directly benefit each other. Indeed, when the generalist *Red* is added to a system with polluter *Blue* and a cleaner *Green*, the cleaner *Green* goes extinct and the biomass of the polluter *Blue* decreases (inset). Nevertheless, the steady-state nutrient environment is moved from a cyan dot lying inside the maximal growth contour to the purple dot lying on the maximal growth contour. In the environment of the cyan dot created by cleaner *Green* and polluter *Blue*, *Blue* is not on the top of the fitness landscape of the polluter class (Fig 6F, upper box). By contrast, for the fitness landscape created by polluter *Blue* and generalist *Red* (Fig 6F, lower box), despite being lower in biomass, *Blue* occupies the top of the landscape. Therefore, the optimal coexistence of this polluter and this generalist does not arise from direct cooperation, but rather from collaborating to defeat other competitors.

DISCUSSION

The phrase "survival of the fittest" used to describe natural selection can be applied both to competition within species and to species competing in the same environment. One doctrine governing resource competition among species is the competitive exclusion principle: theoretically, there should be no more surviving species than the number of resources. However, the enormous diversity of coexisting species in the natural world seems to contradict the competitive exclusion principle. This so-called “paradox of the plankton” has stimulated many theoretical models of resource competition, each with its own assumptions and different conclusions. In this work, we examined a range of models for metabolic competition among microbes within a unified framework, using the species-environment feedback as an organizing principle and the geometric “rule of invasion” and dynamic fitness landscapes as common tools. Under this unified framework, it becomes apparent how metabolic tradeoffs promote diversity by allowing a dynamic fitness landscape without a fittest peak. The implications of non-static landscapes have been under discussion (de Visser, Elena, Fragata, & Matuszewski, 2018) ever since the introduction of fitness landscapes by Wright (Wright, 1932). Nonetheless, in most of these studies, variability in fitness is introduced by externally-imposed environmental fluctuations (Mustonen & Lässig, 2009; Zhang, 2012). In our work, we focused on how fitness landscapes can be intrinsically dynamic due to species’ own actions on their environment.

Graphical representations of resource-competition models are not new. The school of contemporary niche theory dates back almost 50 years (MacArthur, 1970; David Tilman, 1980, 1982), and the growth contours in our work reduce to the zero-net growth isoclines (ZNGI) introduced by this school in the particular case of two growth-promoting resources. Our framework, nonetheless, differs in several aspects: First, we focused on metabolic models with trade-offs, for which there are not only different ZNGIs for different species but a continuous family of growth contours, and the envelope of all growth contours is the maximal growth contour. Given these resource allocation trade-offs, the growth contours of any pair of species must intersect, clearly demonstrating why metabolic trade-offs prevent a single species from unconditional dominance. Moreover, the definition of growth contours is not limited by the number of resources, nor constrained by whether external chemical concentrations contribute positively or negatively to growth, making the approach suitable to address more realistic metabolic models. Second, the introduction of the flux-balance curve, in additional to the supply line, makes it easier to determine the species-specific environment for a given supply condition, which is particularly useful for determining the non-invasible environment as the intersection between maximal growth contour and the maximal flux-balance curve. In brief, our new graphical approach is well suited to our goals of understanding coexistence from the perspective of species-environment feedback, demonstrating how the fitness landscape is changed by the species present, and identifying evolutionarily stable strategies.

Our work is not aimed at adding another solution to the paradox of the plankton. Rather we provide a graphic tool to unify several approaches, and suggest how different

proposed solutions to the paradox can emerge intrinsically from competition for resources. When nutrients are substitutable, resource competition among species with metabolic trade-offs has been shown to lead to emergent neutrality (Posfai et al., 2017), as the fitness landscape is made flat by the competing species. Other commonly invoked solutions to the paradox of the plankton are extrinsic temporal and/or spatial heterogeneity. In this work, we showed that both types of heterogeneity can also emerge intrinsically from species-environment feedback. When the rule of invasion allows non-transitive loops, oscillations and chaos can occur, which have been shown to allow coexistence beyond competitive exclusion (Huisman & Weissing, 1999, 2001). In addition, when multiple nutrients are all essential, the ability of each species to create an environment that favors itself allows for the spontaneous emergence of spatial heterogeneity in an extended system (Fig S2).

Yet, even if fixed species can coexist in an ecosystem, will coexistence survive the ceaseless process of mutation and adaptation? Our approach provides a general protocol to determine non-invasible/evolutionarily stable metabolic strategies, which we demonstrate in the context of three different metabolic models. In these examples, there is a unique non-invasible solution at the intersection of the maximal growth contour and the maximal flux-balance curve. Nevertheless, other models for species competition suggest multiple or, in some cases, zero evolutionarily stable outcomes. For example, in a metabolic model with multiple essential nutrients, Goyal et al. (Goyal, Dubinkina et al. 2018) found multistability in a discrete strategy space, with each steady state non-invasible. By contrast, a study based on a Lotka-Volterra model (in which resource competition is taken to contribute to direct interactions between species (Letten et al., 2017)) found that evolution via continuous introduction of new species drives the system into an chaotic state with a large number of species, i.e. coexistence without a steady state (Ackland & Gallagher, 2004). In the future it will be worthwhile to employ graphical approaches to investigate what types of metabolic models with various shapes of growth contours and flux-balance curves can lead to such non-unique non-invasible outcomes of resource competition.

Another advantage of our graphical approach, besides providing an intuitive picture of species competition, is that it can help understand and control nutrient limitation in chemostat experiments. The capacity of species to shape their own environment, even in a system as simple as a chemostat, presents challenges to controlling which nutrient or nutrients are limiting. By traditional definition, if increasing a certain nutrient leads to an increase of a cell's growth rate, that nutrient is considered "limiting". However, growth rate is invariant in a chemostat, being set experimentally by the dilution rate, so inferring nutrient limitation requires special attention. For example, if one sees the same cellular responses under different nutrient supplies, what can one conclude? Cells may be creating the same nutrient environment out of different supply conditions (*cf*. Fig 1D), or alternatively cells may be transducing different nutrient environments into the same physiological response through mechanisms such as "ratio sensing" (Escalante-Chong et al., 2015). Our graphical approach combined with direct measurements of steady-state nutrient concentrations in the chemostat can precisely define and help control nutrient limitation (Boer, Crutchfield, Bradley, Botstein, & Rabinowitz, 2010)(Boer et al.,

2010). As described above, changes in supply concentrations shift the flux-balance curve, but do not change the shape of the growth contour. Therefore, by experimentally varying the supply conditions and measuring the nutrient environment created by cells, the shape of the growth contour can be obtained. The resulting slope of the growth contour provides information on nutrient limitation even in the absence of detailed knowledge about a cell's metabolism. For example, in the nutrient *a* - nutrient *b* plane, a near-horizontal growth contour indicates *b*-limited growth while a near-vertical growth contour means *a*-limited growth, and an intermediate slope implies that the two nutrients are co-limiting.

Many future directions can follow this work. From the perspective of experiment, our framework can assist in analyzing and interpreting results of microbial evolution in the lab (Van den Bergh, Swings, Fauvart, & Michiels, 2018), where the continual emergence of new mutants under defined experimental conditions suggests an intrinsically dynamic fitness landscape. From the perspective of theory, we do not yet have a rigorous mathematical theorem about the conditions for discontinuity of the maximal growth contour, nor proof that discontinuity necessarily leads to evolutionarily stable coexistence. Theoretical developments paralleling those on the general existence of ecologically stable states (De Leenheer, Levin, Sontag, & Klausmeier, 2006; Marsland III, Cui, & Mehta, 2019) would bring a more comprehensive understanding of evolutionarily optimal states in metabolic models. Besides, the metabolic models considered in this work are highly simplified. Going forward, more detailed and experimentally-based models can be examined using the same graphical framework.

METHODS

Programs for this work is coded in MATLAB R2018a. A repository of all tools used to generate results in this program can be found at:
https://github.com/zhiyuanli1987/Qbiotoolbox.git

Total RNA and total protein measurements

The method for total RNA and protein measurements is described in (Li et al., 2018).

Supplemental Table 1: Symbols

Chemostat parameters	
$\vec{c}_{\text{supply}} = (c_{1,\text{ supply}}, c_{2,\text{ supply}}, \dots c_{p,\text{ supply}})$	Nutrient supply. $c_{i,\text{ supply}}$ is the concentration of the i-th nutrient in the supply.
d	Dilution rate (same as supply influx rate to keep volume fixed).
Chemostat variables	
$\vec{c}_k = (c_{1,k}, c_{2,k}, \dots c_{p,k})$	Nutrient environment inside the k-th chemostat. $c_{i,k}$ is the concentration of the i-th nutrient within the medium of the k-th chemostat. All possible $\vec{c}$ constitute the "nutrient space".
$m_{\sigma,k}$	Biomass density of species σ in the k-th chemostat.
Species-specific quantities	
$\vec{\alpha}_\sigma = (\alpha_{1,\sigma}, \alpha_{2,\sigma} \dots)$	Resource allocation strategy of species σ. $\alpha_{j,\sigma}$ is the fraction of resources allocated to the j-th cellular function by species σ.
$\vec{q}_\sigma$	Intracellular concentrations of growth-related metabolites for species σ.
$g(\vec{c}, \vec{q}, \vec{\alpha})$	Growth rate as a function of $\vec{c}$, $\vec{q}$, and $\vec{\alpha}$.
$I_i(\vec{c}, \vec{q}, \vec{\alpha})$	Intake rate per biomass of the i-th nutrient as a function of $\vec{c}$, $\vec{q}$, and $\vec{\alpha}$. $I_i(\vec{c}, \vec{q}, \vec{\alpha})$ can be negative to describe cells exporting secondary metabolites.
r	Biomass concentration within a cell, taken to be a constant that always equal to 100.
$\vec{f}(\vec{I}(\vec{c}, \vec{q}, \vec{\alpha}), \vec{q}, \vec{\alpha})$	Functions defining the changing rate of intracellular metabolite concentrations $\vec{q}$, as a function of $\vec{c}$, $\vec{q}$, and $\vec{\alpha}$.
GC_σ	Growth-rate contour of species σ.
FB_σ	Flux-balance curve of species σ.
$\vec{c}_{\sigma,\text{ ss}}$	The steady-state environment created by one species σ.

$SL_\sigma(\vec{c})$	The supply line for species σ in environment $\vec{c}$.
$\{\sigma^*\}$	A set of species stably surviving in chemostat. A set can contain one or more species.
$\vec{c}_{\{\sigma^*\},\mathrm{ss}}$	The steady-state environment created by a set of species $\{\sigma^*\}$.

Metabolic model and resource allocation strategy

In modeling population dynamics in a chemostat, multiple assumptions need to be made concerning how cells sense the environment, import nutrients, export metabolites, utilize resources, and grow in biomass. Different assumptions result in different metabolic models. Some metabolic models focus on trade-offs in resource allocation, as the amount of resources "owned" by a cell, including proteins and energy, is limited. Cells need to allocate these limited resources into different cellular functions, such as metabolism, gene expression, reproduction, motility, maintenance, etc. We use $\alpha_{j,\sigma}$ to represent the fraction of resources allocated to the j-th cellular function of species σ, with $\vec{\alpha}_\sigma = (\alpha_{1,\sigma}, \alpha_{2,\sigma} \ldots)$ representing the resource allocation strategy of species σ. For simplicity, we assume each species has a fixed resource allocation strategy.

Dynamic equations for a single species in a chemostat

In a chemostat with nutrient supply $\vec{c}_{\mathrm{supply}}$, dilution rate d and a single species σ with fixed strategy $\vec{\alpha}_\sigma$ and intracellular metabolite concentration $\vec{q}_\sigma$, the cell biomass density m_σ and the chemostat nutrient concentrations $\vec{c}$ are generally described by the following equations:

$$\frac{dm_\sigma}{dt} = m_\sigma \cdot (g(\vec{c}, \vec{q}_\sigma, \vec{\alpha}_\sigma) - d), \quad \textbf{(S1)}$$

$$\frac{d\vec{c}}{dt} = d \cdot \left(\vec{c}_{\mathrm{supply}} - \vec{c}\right) - m_\sigma / r \cdot \vec{I}(\vec{c}, \vec{q}_\sigma, \vec{\alpha}_\sigma). \quad \textbf{(S2)}$$

In considering the details of cellular metabolism, one may choose to incorporate the dynamics of intracellular metabolites that originate from nutrient import and influence cell growth. We make the assumption that the biomass concentration r, e.g. protein concentration, is constant for cells under all growth conditions. Thus, an increase of total cell mass induces a linear increase of total cell volume. m_σ is the cell mass per volume in the chemostat, and r is the cell mass per volume within a cell. For a chemostat-to-cell flux of mass J, the concentration of the metabolite in chemostat decrease by $J/V_{chemsotat}$ while the concentration in cell increase by J/V_{cell}. As a result, the metabolites imported into cells are enriched by a factor of r, and metabolites secreted by cells are diluted by $1/r$. Also, all metabolites are diluted by cellular growth, which is generally a slow process compared to metabolic reactions and can be ignored in most cases. We use a function $\vec{f}(\vec{I}(\vec{c}, \vec{q}, \vec{\alpha}), \vec{q}, \vec{\alpha})$ to represent the rate of change of intracellular metabolite $\vec{q}_\sigma$:

$$\frac{d\vec{q}_\sigma}{dt} = \vec{f}\left(\vec{I}(\vec{c}, \vec{q}_\sigma, \vec{\alpha}_\sigma), \vec{q}_\sigma, \vec{\alpha}_\sigma\right). \quad \textbf{(S3)}$$

Where Eq. (S2) represents p equations for p types of nutrients, and Eq. (S3) represents h equations for h growth-related intracellular metabolites.

Species-specific steady state

In the steady state of chemostat, Eqs. (S1)- (S3) should be all equal to zero. For intracellular metabolites, as $\vec{f}\left(\vec{I}(\vec{c},\vec{q}_\sigma,\vec{\alpha}_\sigma),\vec{q}_\sigma,\vec{\alpha}_\sigma\right)=0$ as a result of Eq. (S3)=0, given an environment $\vec{c}$, the steady state of $\vec{q}_\sigma$ can be expressed as a function of $\vec{c}$: $\vec{q}_\sigma^{*}=\vec{f}^{-1}(\vec{c},\vec{\alpha}_\sigma)$.

Growth contour (GC): From the perspective of the environment influencing species, at each constant environment, the steady-state growth rate is fully determined by $\vec{c}$: $g^*(\vec{c},\vec{q}_\sigma)=g\left(\vec{c},\vec{f}^{-1}(\vec{c},\vec{\alpha}_\sigma)\right)$. If the biomass of a species is non-zero ($m\neq 0$), Eq. (S1) requires $g^*=d$. In the p-dimensional nutrient space, this requirement defines a $(p-1)$-dimensional surface, constituted by all environments $\vec{c}$ that support an equal-to-dilution growth rate. This surface reduces to the zero-growth isoclines in contemporary niche theory when the nutrient space is two-dimensional and the growth rate g solely relies on $\vec{c}$ monotonically, but is not necessarily limited by the nutrient dimension or the form of the growth function. For convenience, we name this surface the "growth contour" (GC) for species σ:

$$GC_\sigma \coloneqq \{\vec{c}\mid g\left(\vec{c},\vec{f}^{-1}(\vec{c},\vec{\alpha}_\sigma),\vec{\alpha}_\sigma\right)=d\}. \quad \textbf{(S4)}$$

An example of growth contours is shown in Fig 1D.

Flux-balance curve (FB): Eq. (S2) describes how species act on the environment. In steady state, the influx, out-flux, and consumption by species should be balanced for each nutrient, which enables calculation of the biomass density-to-dilution ratio for every i: $\frac{m_\sigma}{d\cdot r}=\frac{c_{i,\,\mathrm{supply}}-c_i}{I_i\left(\vec{c},\vec{f}^{-1}(\vec{c},\vec{\alpha}_\sigma),\vec{\alpha}_\sigma\right)}$. For a p-dimensional nutrient space, there are p equations for the same value of $\frac{m}{d\cdot r}$. This leads to a one-dimensional curve in the nutrient space, which we name the "flux-balance curve" (FB), defined as:

$$FB \coloneqq \{\vec{c}\mid \frac{c_{i,\,\mathrm{supply}}-c_i}{I_i\left(\vec{c},\vec{f}^{-1}(\vec{c},\vec{\alpha}_\sigma),\vec{\alpha}_\sigma\right)}=\frac{m_\sigma}{d\cdot r}\ \mathrm{AND}\ c_i<c_{i,\mathrm{supply}}\}. \quad \textbf{(S5)}$$

For example, for two nutrients *a* and *b*, the flux balance curve is: $\frac{c_{a,\,\mathrm{supply}}-c_a}{I_a\left(\vec{c},\vec{f}^{-1}(\vec{c},\vec{\alpha}_\sigma),\vec{\alpha}_\sigma\right)}-\frac{c_{a,\,\mathrm{supply}}-c_a}{I_a\left(\vec{c},\vec{f}^{-1}(\vec{c},\vec{\alpha}_\sigma),\vec{\alpha}_\sigma\right)}=0$, as demonstrated in Fig 1D.

In nutrient space, the steady-state environment ($\vec{c}_{\sigma,\mathrm{ss}}$) with non-zero biomass of species σ will be located at the intersection of the growth contour and the flux-balance curve. This environment is constructed by the species σ via its consumption of nutrients. If $\vec{c}_{\sigma,\mathrm{ss}}$ exists, this species can survive in the chemostat. Otherwise, this species will be washed out by dilution even without competition from other species. For the following discussion, we only consider species that can survive when alone in a chemostat.

Supply line (SL): The flux-balance curve is determined by the supply condition $\vec{c}_{\mathrm{supply}}$. In many cases, it is helpful to derive the supply conditions that enable a species σ to construct a steady-state environment $\vec{c}_{\sigma,\mathrm{ss}}$. All possible values of $\vec{c}_{\mathrm{supply}}$ that can produce a given $\vec{c}_{\sigma,\mathrm{ss}}$, form a straight line in the space of supply concentrations, described by:

$$SL \coloneqq \{\vec{c}_{\mathrm{supply}}\mid \vec{c}_{\mathrm{supply}}=\frac{m_\sigma}{d\cdot r}\cdot\vec{I}\left(\vec{c}_{\sigma,\mathrm{ss}},\vec{f}^{-1}\left(\vec{c}_{\sigma,\mathrm{ss}},\vec{\alpha}_\sigma\right),\vec{\alpha}_\sigma\right)+\vec{c}_{\sigma,\mathrm{ss}}\}, \quad \textbf{(S6)}$$

with varying non-negative values of m_σ/d. An example of a supply line is shown in Fig 1D.

Dynamic equations for multiple species in a chemostat

In nutrient competition models, multiple species ($\sigma = 1 \ldots n$) each with biomass density m_σ compete for resources. They have species-specific growth rates $g(\vec{c}, \vec{q}_\sigma, \vec{\alpha}_\sigma)$ and import rates $\vec{I}(\vec{c}, \vec{q}_\sigma, \vec{\alpha}_\sigma)$, yet all experience the same nutrient environment $\vec{c}$. Therefore, Eq. (S1) and Eq. (S3) remain the same for each species, while the rate of change of chemostat nutrient concentrations is influenced by the summed action of all species:

$$\frac{d\vec{c}}{dt} = d \cdot \left(\vec{c}_{\text{supply}} - \vec{c}\right) - \sum_{\sigma=1}^{n} m_\sigma/r \cdot \vec{I}(\vec{c}, \vec{q}_\sigma, \vec{\alpha}_\sigma). \quad \textbf{(S7)}$$

Multiple species steady state

Multiple species, even if each alone can survive in chemostat, do not generally coexist when competing together. For a system starting with n different species, the stable steady state contains n^* ($1 \le n^* \le n$) species with non-zero biomass. We define these n^* surviving species as a stable species set $\{\sigma^*\}$, and mark the steady-state environment created by this set as $\vec{c}_{\{\sigma^*\},\text{ss}}$. If $n > 1$, according to Eq. (S1), $\vec{c}_{\{\sigma^*\},\text{ss}}$ must be located at the common intersection of growth contours formed by every species in $\{\sigma^*\}$.

Invasion

Invasion is defined as introducing a small number of invaders (with biomass density m_{inv}) to a steady-state chemostat occupied by a set of local species. At the time of introduction, if the invader can increase in biomass ($\frac{dm_{\text{inv}}}{dt} > 0$), the invasion is successful; otherwise if the invader decreases in biomass ($\frac{dm_{\text{inv}}}{dt} < 0$), the invasion is unsuccessful. If the biomass stays constant ($\frac{dm_{\text{inv}}}{dt} = 0$), the species is neutral with respect to the local species.

In evaluating invasion by a species σ with strategy $\vec{\alpha}_\sigma$ of any environment $\vec{c}$, we make two assumptions:

1. The biomass of the invader is so small that it does not disturb the environment at the time of introduction.
2. There is a separation of timescales such that the concentrations of intracellular metabolites reach equilibrium instantaneously at the time of introduction of the invader, therefore Eq. (S3) is always equal to zero and $\vec{q}_\sigma = \vec{f}^{-1}(\vec{c}, \vec{\alpha}_\sigma)$ holds.

Therefore, we define the "invasion growth rate" of a species σ with strategy $\vec{\alpha}_\sigma$ introduced into environment $\vec{c}$ as:

$$g_{\text{inv}}(\vec{\alpha}|\vec{c}) = g\left(\vec{c}, \vec{f}^{-1}(\vec{c}, \vec{\alpha}), \vec{\alpha}\right). \quad \textbf{(S8)}$$

Invasion zone: By definition, the growth contour of the invader GC_{inv} divides the nutrient space into two regions: an "invasion zone" that includes all environments where the invader has an invasion growth rate higher than dilution, and "no-invasion zone" where the invader has an invasion growth rate lower than dilution. If the steady-state environment constructed by local species $\vec{c}_{\{\text{local}\},\text{ss}}$ is located within the invasion zone of

the invader, $g_{\mathrm{inv}}\left(\vec{\alpha}_{\mathrm{inv}}|\vec{c}_{\{\mathrm{local}\},\mathrm{ss}}\right) > d$, therefore $\frac{dm_{\mathrm{inv}}}{dt} > 0$ by Eq. (S1), and the invasion is successful; otherwise, if $\vec{c}_{\{\mathrm{local}\},\mathrm{ss}}$ is located outside of the invasion zone of the invader, $g_{\mathrm{inv}}\left(\vec{\alpha}_{\mathrm{inv}}|\vec{c}_{\{\mathrm{local}\},\mathrm{ss}}\right) < d$, and the invasion is unsuccessful. If $\vec{c}_{\{\mathrm{local}\},\mathrm{ss}}$ locate exactly on the growth contour, it is neutral.

Two examples of this rule of invasion are presented in Fig 2A and 2B.

If the growth rate monotonically increases with the concentration of each nutrient, it can be proven that the invasion zone is always above the growth contour of the invader (an environment $\vec{c}_+$ "above" the growth contour GC_{inv} is defined as $\exists \vec{c}_0 \in GC_{\mathrm{inv}}, \mathrm{s.t.}\ c_{i,+} \geq c_{i,0}\ \forall\ i$). If the growth rate is not monotonically increasing with nutrient concentrations, identifying the invasion zone requires more model-specific analysis.

Fitness landscape

We quantified the fitness landscapes in the chemostat via the relationship between metabolic strategies $\vec{\alpha}$ and the invasion growth rates of an invader adopting strategy $\vec{\alpha}$ in a given nutrient environment $\vec{c}$. Specifically,

$$Fitness\ landscape \coloneqq g_{\mathrm{inv}}(\vec{\alpha}|\vec{c}). \qquad \textbf{(S9)}$$

Each environment $\vec{c}$ defines a fitness landscape. A set of species $\{\sigma^*\}$ constructs a steady-state environment $\vec{c}_{\{\sigma^*\},\mathrm{ss}}$ and a corresponding fitness landscape $g_{\mathrm{inv}}\left(\vec{\alpha}|\vec{c}_{\{\sigma\},\mathrm{ss}}\right)$. Some examples of fitness landscapes are shown in Figs 2D, 3C, 4B-C, 5D and 6D-F.

Non-invasible /optimal/ evolutionarily stable strategies

A set of species $\{\sigma^*\}_{\mathrm{opt}}$ is non-invasible, aka optimal or evolutionarily stable, if no other species can invade the steady-state environment constructed by $\{\sigma^*\}_{\mathrm{opt}}$:

$$g_{\mathrm{inv}}\left(\vec{\alpha}_\sigma|\vec{c}_{\{\sigma^*\}_{\mathrm{opt}},\mathrm{ss}}\right) < d\ ,\forall\ \sigma \notin \{\sigma^*\}_{\mathrm{opt}}. \qquad \textbf{(S10)}$$

Equivalently, Eq. (S10) can be expressed as "a set of species $\{\sigma^*\}_{\mathrm{opt}}$ construct a fitness landscape which places themselves on the top", according to Eq. (S9).

The steady state constructed by $\{\sigma^*\}$ is influenced by the supply $\vec{c}_{\mathrm{supply}}$ and the dilution rate d. For different chemostat parameters, the non-invasible species set $\{\sigma^*\}_{\mathrm{opt}}$ may be different. In the following steps, we described a generally applicable protocol for obtaining the non-invasible strategies:

1. Maximal growth rates and maximizing strategies: In a metabolic model with trade-offs in resource allocation, the maximizing resource allocation strategy $\vec{\alpha}_{\mathrm{max}}$ under a given environment $\vec{c}$ is defined as the strategy that maximizes invasion growth rate:

$$g_{\mathrm{max}}(\vec{c}) \coloneqq \max_{\vec{\alpha}}\left(g_{\mathrm{inv}}(\vec{\alpha}_\sigma|\vec{c})\right) \qquad \textbf{(S11)}$$
$$\vec{\alpha}_{\mathrm{max}}(\vec{c}) \coloneqq \arg\max_{\vec{\alpha}}\left(g_{\mathrm{inv}}(\vec{\alpha}_\sigma|\vec{c})\right).$$

2. Maximal growth contour: For a given dilution rate d, all environments that support a maximal growth rate of d constitute the "maximal growth contour":

$$GC_{\max} \coloneqq \{\vec{c}_0 \mid g_{\max}(\vec{c}_0) = d\}. \quad \textbf{(S12)}$$

$GC_{\max}$ is generally formed by many species, with each species adopting the maximizing strategies $\vec{\alpha}_{\max}(\vec{c}_0)$ corresponding to one environment $\vec{c}_0$ on the maximal growth contour.

$GC_{\max}$ is outside of the invasion zone for any species σ. (Otherwise, if a species σ could invade an environment $\vec{c}_0$ on $GC_{\max}$, $g_{\text{inv}}(\vec{\alpha}_\sigma|\vec{c}_0 \in GC_{\max}) > d$, this would directly violate the requirement by Eqs. (S11) and (S12) that $\max_{\vec{\alpha}}\left(g_{\text{inv}}(\vec{\alpha}_\sigma|\vec{c}_0)\right) = d$.) Therefore, the necessary and sufficient condition for a set of species to be evolutionarily stable, is to construct a steady-state environment on the maximal growth contour:

$$\vec{c}_{\{\sigma^*\}_{\text{opt}},\text{ss}} \in GC_{\max}. \quad \textbf{(S13)}$$

Therefore, a strategy belonging to the non-invasible set must be a maximizing strategy. An example of maximal growth contour is shown in Fig 4D.

3. Non-invasible strategy: Nevertheless, adopting one of the maximizing strategies along the maximal growth contour does not guarantee that a species will satisfy Eq. (S13) and become non-invasible, as a maximizing strategy for environment $\vec{c}_1$ may end up constructing a different environment $\vec{c}_2$. To identify a non-invasible species for supply condition $\vec{c}_{\text{supply}}$, the flux-balance condition needs to be considered, with the strategies maximized at each environment. This requirement forms a "maximal flux-balance curve" in the nutrient space:

$$FB_{\max} \coloneqq \{\vec{c} \mid \frac{c_{i,\,\text{supply}} - c_i}{I_i\left(\vec{c}, \vec{f}^{-1}\left(\vec{c}, \vec{\alpha}_{\max}(\vec{c})\right), \vec{\alpha}_{\max}(\vec{c})\right)} = \frac{m}{d \cdot r} \text{ AND } c_i < c_{i,\text{supply}}\}. \quad \textbf{(S14)}$$

If the intersection of the maximal growth contour and the maximal flux-balance curve exists, it is the evolutionarily stable environment under dilution rate d and supply condition $\vec{c}_{\text{supply}}$, $\vec{c}_{\text{opt}}$.The maximizing strategy for this environment, $\vec{\alpha}_{\text{opt}} = \vec{\alpha}_{\max}\left(\vec{c}_{\text{opt}}\right)$, constructs the environment $\vec{c}_{\text{opt}}$, and is evolutionarily stable.

4. Evolutionarily stable coexistence at the discontinuous points of the maximal growth contour: Inversely, for each environment $\vec{c}_0$ on the maximal growth contour, all supply conditions that enables the maximizing strategy of $\vec{c}_0$ to become the non-invasible strategy can be calculated from the supply line according to Eq. (S6):

$$SL(\vec{c}_0) \coloneqq \{\vec{c}_{\text{supply}} \mid \vec{c}_{\text{supply}} = x \cdot \vec{I}\left(\vec{c}_0, \vec{f}^{-1}\left(\vec{c}_0, \vec{\alpha}_{\max}(\vec{c}_0)\right), \vec{\alpha}_{\max}(\vec{c}_0)\right) + \vec{c}_0\}, \quad \textbf{(S15)}$$

for any non-zero value of x. Some examples are shown in Fig 4D.

When there are discontinuous points on the maximal growth contour, there can be "gaps" in the nutrient supply space, where no single strategy on the maximal growth contour satisfies Eq. (S14) . Under this condition, more than one strategy are required to co-create an environment on the conjunctions of discontinuous points of the maximal growth contour. Therefore, discontinuous points of the maximal growth contour permit evolutionarily stable coexistence, where $\{\sigma^*\}_{\text{opt}}$ contains more than one species. Two examples of such discontinuities and coexistence are shown in Fig 5 and Fig 6.

Metabolic models

Different assumptions can be made regarding the metabolic models $\vec{f}(\vec{c},\vec{x},\vec{\alpha})$, $g(\vec{c},\vec{x},\vec{\alpha})$, and $\vec{I}(\vec{c},\vec{x},\vec{\alpha})$, focusing on various aspects of cellular growth. Different assumptions lead to distinct classes of metabolic models with various results. Nevertheless, our analysis schemes, including the invasion geometry, fitness landscape, and evolutionary stable strategies, are generally applicable for various metabolic models. In this work, we used five metabolic models to illustrate multiple aspects of the species-environment feedback:

1. Metabolic model with two essential nutrients

When two nutrients are both essential for growth, such as nitrogen and phosphorus, and both require a substantial allocation of resources for import, the system can be abstractly modeled as shown in Fig 4A. In this metabolic model, we assume an exact trade-off between the allocation of limited resources to import nutrient *a* or nutrient *b*. The fraction of resources allocated to import nutrient *a* is represented by α_a, thus leaving a fraction $\alpha_b = 1 - \alpha_a$ to import nutrient *b*. The import rate of nutrient i is assumed to follow the Monod equation as a function of nutrient concentration, and is proportional to α_i:

$$I_i(\vec{c}) = \alpha_i \cdot \frac{c_i}{c_i + K_i} \text{ for } i = a, b. \quad \textbf{(S16)}$$

Import of both nutrients is required for cell growth:

$$g(\vec{c}) = \gamma \cdot \min(I_a(\vec{c}), I_b(\vec{c})). \quad \textbf{(S17)}$$

For this model, for simplicity we do not explicitly consider intracellular metabolites. Rather, import directly determines growth.
In this model, a "species" is defined by its value of α_a.
Nutrient limitation can be clearly quantified in this system: if $I_a(\vec{c}) > I_b(\vec{c})$, the system is limited by nutrient *b*; if $I_a(\vec{c}) < I_b(\vec{c})$, the system is limited by nutrient *a*.

A species with the following parameters was used to generate Fig 1D and E, focusing on how supply conditions and dilution rate influence nutrient limitation:

K_a	K_b	γ	α_a
0.7	1.3	10	0.3

In Fig 1D, to demonstrate how species construct the same environment out of different supply conditions, the chemostat dilution rate was set to $d = 1$, and three supply conditions were used: $\vec{c}_{\text{supply}} = [0.6, 0.3546]$ (purple), $\vec{c}_{\text{supply}} = [0.8, 0.5273]$ (cyan), and $\vec{c}_{\text{supply}} = [1, 0.7]$ (blue).
In Fig 1E, to demonstrate how dilution rates may switch the nutrient, we used the same supply condition as the blue condition in Fig 1D ($\vec{c}_{\text{supply}} = [1, 0.7]$), and three dilution rates: 0.5 (yellow), 1 (red), and 1.6 (deep red).

Species with following parameters were used to generate Fig 4B-D:

K_a	K_b	γ
0.5	0.5	10

The strategy α_a varies for different species. In Fig 4B, Species *Blue* has $\alpha_a = 0.35$, species *Red* has $\alpha_a = 0.65$. In Fig 4C, we started with species *Blue* and species *Red*.

We then generated the fitness landscape for each species at the steady-state environment it constructed, then chose the strategy that maximized invasion growth rate for this fitness landscape to generate a new species, and iterated this process five times. The species *Black* has $\alpha_a = 0.5$.
In generating Fig 4D, we followed the protocols described in section "Non-invasible / evolutionarily stable strategies".

2. Metabolic model with substitutable nutrients

When two nutrients are mutually substitutable for growth, such as glucose and galactose, the system can be described by metabolic model as shown in Fig 2A. The trade-off and import functions are taken to be the same as in Model 1: *metabolic model with two essential nutrients*. However, import of the two nutrients contributes additively toward growth rate:

$$g(\vec{c}) = \gamma \cdot (I_a(\vec{c}) + I_b(\vec{c})). \quad \textbf{(S18)}$$

A species is defined by its value of α_a.
For this model, all growth contours intersect at one point. The growth contour of species σ satisfies the equation: $\alpha_a \cdot \frac{c_a}{c_a+K_a} + (1-\alpha_a) \cdot \frac{c_b}{c_b+K_b} = d/\gamma$. Regardless of the value of α_a, the environment $[\frac{K_a}{\frac{\gamma}{d}-1}, \frac{K_b}{\frac{\gamma}{d}-1}]$ is always on the growth contour.
Species with the following parameters were used to generate Fig 2B-E:

K_a	K_b	γ
1.2	0.8	3

The strategy α_a varies for different species. In Fig 2B-D, Species *Blue* has $\alpha_a = 0.2$, species *Red* has $\alpha_a = 0.6$. Supply conditions are different among the three figures: in Fig 2B, $\vec{c}_{\text{supply}} = [0.5,1]$; in Fig 2C, $\vec{c}_{\text{supply}} = [1, 0.5]$; in Fig 2D, $\vec{c}_{\text{supply}} = [1,1]$.
All conditions in Fig 2E are the same as in Fig 2D, other than that five additional species are added to the system. Their strategies are indicated by the legend at the right.

3. Metabolic model with substitutable nutrients that require assimilation

In cells, the assimilation of imported raw material, such sugars, into biomass such as proteins, takes multiple steps and enzymes and consumes a considerable amount of energy. When the resources allocated to nutrient assimilation are considered, a cell's strategy becomes more complex. A mathematical model involving three substitutable nutrients *a, b, c* that need assimilation is shown in Fig 3A, with α_{i1} represents the fraction of resources allocated to importing nutrient *i* into internal metabolite, and α_{i2} represents the fraction of resources allocated to assimilate the internal *i* into biomass. In this model, the import rate has a similar form to the previous two models,

$$I_i(c_i) = V \cdot \alpha_{i1} \cdot \frac{c_i}{c_i+K_i}. \quad \textbf{(S19)}$$

The internal metabolite concentration $c_{i,\text{internal}}$ has an influx of $r \cdot I_i(c_i)$, meanwhile, it is diluted by cell growth in the rate of g. We assume all nutrients are substitutable therefore the internal pools contributes via summation to growth, it is converted into biomass at a rate $k \cdot \alpha_{i2} \cdot c_{i,\text{internal}}$:

$$\frac{dc_{i,\text{internal}}}{dt} = I_i(c_i) - g(\vec{c}_{\text{internal}}) \cdot c_{i,\text{internal}} - k \cdot \alpha_{i2} \cdot c_{i,\text{internal}}. \quad \textbf{(S20)}$$

Therefore, the mass converted into biomass per unit time per unit volume is: $\sum_i(k \cdot \alpha_{i2} \cdot c_{i,\mathrm{internal}})$, and the growth rate defined as the relative gain of total biomass *M* is:

$$g(\vec{c}_{\mathrm{internal}}) = \frac{\frac{dM}{dt}}{M} = \frac{k}{r} \cdot \sum_i(\alpha_{i2} \cdot c_{i,\mathrm{internal}}). \quad \textbf{(S21)}$$

In generating Fig 4B-C, the chemostat parameters were: $\vec{c}_{\mathrm{supply}} = [1,1,1]$, and $d = 1$, and the species parameters were:

V	$K_i\ (i = a, b, c)$	k
1000	0.5	11

The three species allocate their resources differently:

Strategies	α_{a1}	α_{a2}	α_{b1}	α_{b2}	α_{c1}	α_{b2}
Red	0.15	0.2	0.1	0.25	0.26	0.04
Green	0.26	0.04	0.15	0.2	0.1	0.25
Blue	0.1	0.25	0.26	0.04	0.15	0.2

To generate the Fig S1B, all other parameters are the same, other than $k = 10$.

4. Metabolic model with essential nutrients that can be interconverted

If two nutrients are both essential for growth, and a cell is able to convert one nutrient into another albeit at a certain cost, as shown in Fig 5A, metabolic trade-offs involve the following four elements of the allocation strategy $\vec{\alpha}$:

α_a: Fraction of resources allocated to import nutrient *a*.

α_b: Fraction of resources allocated to import nutrient *b*.

α_{ab}: Fraction of resources allocated to convert internal *b* into *a*.

α_{ba}: Fraction of resources allocated to convert internal *a* into *b*.

To implement trade-offs, the sum of elements of $\vec{\alpha} = (\alpha_a, \alpha_b, \alpha_{ab}, \alpha_{ba})$ is taken to be equal to 1.

In this metabolic model, cells internalize nutrient *a* and nutrient *b* from the chemostat to supply internal concentration of nutrients, $c_{a,\mathrm{internal}}$ and $c_{b,\mathrm{internal}}$. Meanwhile, the internal nutrients can be converted into each other. Nutrients also diffuse in and out of the cell passively with rate β. Cell growth requires both internal nutrients, and depletes them in a fixed proportion.

In this model, the growth rate of a cell is taken to be:

$$g(\vec{c}_{\mathrm{internal}}) = \frac{\gamma}{\frac{K_a}{c_{a,\mathrm{internal}}} + \frac{K_b}{c_{b,\mathrm{internal}}}}. \quad \textbf{(S22)}$$

The net import rate, including passive diffusion, is:

$$I_i = (\alpha_i + \beta) \cdot c_i - \beta \cdot c_{i,\mathrm{internal}},\ i = a, b. \quad \textbf{(S23)}$$

Therefore, the dynamical equations for the internal nutrients are:

$$\frac{dc_{a,\mathrm{internal}}}{dt} = I_a + \alpha_{ab} \cdot c_{b,\mathrm{internal}} - \alpha_{ba} \cdot c_{a,\mathrm{internal}} - g/K_a, \quad \textbf{(S24)}$$

$$\frac{dc_{b,\text{internal}}}{dt} = I_b + \alpha_{ba} \cdot c_{a,\text{internal}} - \alpha_{ab} \cdot c_{b,\text{internal}} - g/K_b. \quad \textbf{(S25)}$$

A species is defined by its value of $\vec{\alpha}$.

This metabolic model was used to demonstrate how to obtain locally optimal strategies and cartels, as shown in Fig 5. The parameter values used to generate the plots in Fig 5B-D were:

γ	$K_i\ (i = a, b)$	β
1	1	0.2

In generating Fig 5B, we searched for the maximizing strategies in the nutrient space, and classified them by their non-zero values. Maximal growth contours for four dilution rates: 0.1, 0.2, 0.3, 0.4 are shown from black to gray and white colors.
In generating Fig 5C, the chemostat parameters were set to $\vec{c}_{\text{supply}} = [0.5,1]$, and $d = 0.2$. The maximal growth contours for $d = 0.2$ were drawn, along with maximizing strategies along the contour shown as squares with colors corresponding to their sub-classes. At the discontinuous point of the maximal growth contour where the "converter" and the "importer" converge, the distinct two maximizing strategies are denoted species *Red* and species *Blue*. In generating the competition dynamics in inset, additional to the species *Red* and species *Blue*, ten other maximizing strategies along the maximal growth contours were chosen.

5. Metabolic model with multiple energy generating steps

Cell growth is also tightly coupled with energy production. For example, with a single carbon supply as the energy source, cells employ multi-step reactions to generate multiple ATP molecules. Each step requires dedicated enzymes. The reaction intermediates, such as acetate, usually have dual roles: on the one hand, they positively contribute to ATP production via downstream reactions; on the other hand, they negatively contribute to ATP production by hampering upstream reactions. To deal with the negative effects of intermediates, cells may transport them out into the environment, generally with some metabolic cost for transporters. On the other hand, cells can also uptake such intermediates and use them as an energy source.
We abstract such a process by the model shown in Fig 6A. A single chemical energy source *S* is supplied into the chemostat, which can be converted into intermediate *I* by cells. Four reactions are possible in this model, each mediate by a specific enzyme:
1. Import the resource *S* into the cell and convert it into internal intermediate I_{int} to extract energy (e.g. ATP). The fraction of the model enzyme budget allocated to this reaction is α_{ATP1}. We assume the reaction is reversible, with the concentration *S* contributing positively to the reaction rate while the concentration I_{int} contributes negatively:

$$J_1 = \alpha_{\text{ATP1}} \cdot V_1 \cdot \frac{[S] - \frac{[I_{\text{int}}]}{K_3}}{K_1 + [S] + \frac{[I_{\text{int}}]}{K_5}}. \quad \textbf{(S26)}$$

2. Process I_{int} via a downstream reaction to obtain more energy. The fraction of enzymes being allocated to this reaction is α_{ATP2}. For this model system, it does not

qualitatively influence the final results whether this reaction is product inhibited. For simplicity, we assume this reaction has Michaelis–Menten form:

$$J_2 = \alpha_{\mathrm{ATP2}} \cdot V_2 \cdot \frac{[I_{\mathrm{int}}]}{K_2 + [I_{\mathrm{int}}]}. \quad \textbf{(S27)}$$

3. Export the internal intermediate out into the environment by diffusion, with a fraction of proteins α_{exp} allocated to channels that allow the excretion of the intermediate into the environment to become external intermediate I_{ext}.

$$J_3 = \alpha_{\mathrm{exp}} \cdot k \cdot ([I_{\mathrm{int}}] - [I_{\mathrm{ext}}]). \quad \textbf{(S28)}$$

4. Import the external intermediate into cells, with a fraction of proteins α_{imp} allocated to the import process. In reflect the property of the internal intermediate in inhibiting this transport reaction, the rate for this process is also product-inhibited:

$$J_4 = \alpha_{\mathrm{imp}} \cdot V_4 \cdot \frac{[I_{\mathrm{ext}}] - \frac{[I_{\mathrm{int}}]}{K_6}}{K_4 + [I_{\mathrm{ext}}] + \frac{[I_{\mathrm{int}}]}{K_7}}. \quad \textbf{(S29)}$$

Under this model, the rate of change for the energy source concentration in the chemostat is:

$$\frac{d[S]}{dt} = d \cdot \left([S_{\mathrm{supply}}] - [S]\right) - m/r \cdot J_1 \quad \textbf{(S30)}$$

The rate of change of the external intermediate concentration in the chemostat is:

$$\frac{d[I_{\mathrm{ext}}]}{dt} = d \cdot (-[I_{\mathrm{ext}}]) - m/r \cdot (J_4 - J_3). \quad \textbf{(S31)}$$

The concentration for the intercellular metabolite I_{int} follows the equation:

$$\frac{d[I_{\mathrm{int}}]}{dt} = J_1 - J_2 - J_3 + J_4. \quad \textbf{(S32)}$$

The growth rate is a weighted sum of the ATP produced by J_1 and J_2:

$$g = n_{\mathrm{ATP1}} \cdot J_1 + n_{\mathrm{ATP2}} \cdot J_2. \quad \textbf{(S33)}$$

In generating plots in Fig 6B-F, the species parameters were:

V_1	V_2	k	V_4	K_1	K_2	K_3	K_4	K_5	K_6	K_7	n_{ATP1}	n_{ATP2}
5	1	8	10	0.5	0.5	0.5	0.1	0.5	15	10	1	1

Maximal growth contours for dilution rates 0.2, 0.4, and 0.6 are shown in Fig 6B.
For Fig 6C-D, the chemostat parameters are: $S_{\mathrm{supply}} = 1, d = 0.4$.
For Fig 6E-F, the chemostat parameters are: $S_{\mathrm{supply}} = 1.8, d = 0.6$.

Dynamic equations for multiple species in a chain of chemostats

Real ecosystems seldom exist in isolation. We modeled interconnected ecosystems via a chain of chemostats labeled $k = 1$ to k_{tot} (Fig S2A). Each chemostat exchanges medium and cells at leakage rate l with its two neighboring chemostats (if $k = 1$ or $k = k_{\mathrm{tot}}$, there is only one neighbor). The chemostat parameters $\vec{c}_{\mathrm{supply}}$ and d are taken to be identical for all chemostats.

For the k-th chemostat, the dynamical equations for the biomass density of species σ and the concentration of the i-th nutrient are:

$$\frac{dm_{\sigma,k}}{dt} = m_{\sigma,k} \cdot (g_\sigma(\vec{c}_k) - d) + l \cdot (m_{\sigma,k-1} + m_{\sigma,k+1} - 2 \cdot m_{\sigma,k}), \quad \textbf{(S34)}$$

$$\frac{dc_{i,k}}{dt} = d \cdot \left(c_{i,\,\text{supply}} - c_{i,k}\right) - \sum_{\sigma=1}^{n} m_{\sigma,k} \cdot I_{i,\sigma}(\vec{c}_k) + l \cdot \left(c_{i,k+1} + c_{i,k-1} - 2 \cdot c_{i,k}\right). \quad \textbf{(S35)}$$

A steady-state solution to these equations is shown in Fig S2, using the same growth and import models and parameters as in Fig 4, with the leakage rate set to be $l = 1$.

ACKNOWLEDGEMENTS

We thank Simon Levin for insightful discussions. Zhiyuan Li was supported by Princeton Center for Theoretical Science and Center for the Physics of Biological Function. This work was supported in part by NSF grant PHY-1607612, the National Science Foundation Physics Frontier Center grant through the Center for the Physics of Biological Function (PHY-1734030), and National Institutes of Health Grant (R01 GM082938).

COMPETING INTERESTS

The authors declare that they have no conflict of interest.

REFERENCES

Ackland, G., & Gallagher, I. (2004). Stabilization of large generalized Lotka-Volterra foodwebs by evolutionary feedback. *Physical Review Letters, 93*(15), 158701.

Amarasekare, P. (2003). Competitive coexistence in spatially structured environments: a synthesis. *Ecology Letters, 6*(12), 1109-1122.

Armstrong, R. A., & McGehee, R. (1980). Competitive exclusion. *The American Naturalist, 115*(2), 151-170.

Bairey, E., Kelsic, E. D., & Kishony, R. (2016). High-order species interactions shape ecosystem diversity. *Nat Commun, 7*, 12285. doi:10.1038/ncomms12285

Beardmore, R. E., Gudelj, I., Lipson, D. A., & Hurst, L. D. (2011). Metabolic trade-offs and the maintenance of the fittest and the flattest. *Nature, 472*(7343), 342-346. doi:10.1038/nature09905

Behar, H., Brenner, N., & Louzoun, Y. (2014). Coexistence of productive and non-productive populations by fluctuation-driven spatio-temporal patterns. *Theoretical Population Biology, 96*, 20-29.

Boer, V. M., Crutchfield, C. A., Bradley, P. H., Botstein, D., & Rabinowitz, J. D. (2010). Growth-limiting intracellular metabolites in yeast growing under diverse nutrient limitations. *Mol Biol Cell, 21*(1), 198-211. doi:10.1091/mbc.E09-07-0597

Callahan, B. J., Fukami, T., & Fisher, D. S. (2014). Rapid evolution of adaptive niche construction in experimental microbial populations. *Evolution, 68*(11), 3307-3316. doi:10.1111/evo.12512

Ceballos, G., Ehrlich, P. R., Barnosky, A. D., Garcia, A., Pringle, R. M., & Palmer, T. M. (2015). Accelerated modern human-induced species losses: Entering the sixth mass extinction. *Sci Adv, 1*(5), e1400253. doi:10.1126/sciadv.1400253

Cermeño, P., Teixeira, I. G., Branco, M., Figueiras, F. G., & Marañón, E. (2014). Sampling the limits of species richness in marine phytoplankton communities. *Journal of Plankton Research, 36*(4), 1135-1139.

Chase, J. M., & Leibold, M. A. (2003). *Ecological niches: linking classical and contemporary approaches*: University of Chicago Press.

D'Souza, G., Shitut, S., Preussger, D., Yousif, G., Waschina, S., & Kost, C. (2018). Ecology and evolution of metabolic cross-feeding interactions in bacteria. *Nat Prod Rep, 35*(5), 455-488. doi:10.1039/c8np00009c

De Leenheer, P., Levin, S. A., Sontag, E. D., & Klausmeier, C. A. (2006). Global stability in a chemostat with multiple nutrients. *Journal of Mathematical Biology, 52*(4), 419-438. doi:10.1007/s00285-005-0344-4

de Visser, J., Elena, S. F., Fragata, I., & Matuszewski, S. (2018). The utility of fitness landscapes and big data for predicting evolution. *Heredity (Edinb), 121*(5), 401-405. doi:10.1038/s41437-018-0128-4

Descamps-Julien, B., & Gonzalez, A. (2005). Stable coexistence in a fluctuating environment: an experimental demonstration. *Ecology, 86*(10), 2815-2824.

Escalante-Chong, R., Savir, Y., Carroll, S. M., Ingraham, J. B., Wang, J., Marx, C. J., & Springer, M. (2015). Galactose metabolic genes in yeast respond to a ratio of galactose and glucose. *Proc Natl Acad Sci U S A, 112*(5), 1636-1641. doi:10.1073/pnas.1418058112

1132 Freilich, S., Zarecki, R., Eilam, O., Segal, E. S., Henry, C. S., Kupiec, M., . . . Ruppin, E. (2011).
1133 Competitive and cooperative metabolic interactions in bacterial communities. *Nat*
1134 *Commun, 2*, 589. doi:10.1038/ncomms1597
1135 Friedman, J., Higgins, L. M., & Gore, J. (2017). Community structure follows simple assembly
1136 rules in microbial microcosms. *Nature ecology & evolution, 1*(5), 0109.
1137 Geyrhofer, L., & Brenner, N. (2018). Coexistence and cooperation in structured habitats.
1138 *BioRxiv*, 429605.
1139 Goldford, J. E., Lu, N., Bajić, D., Estrela, S., Tikhonov, M., Sanchez-Gorostiaga, A., . . .
1140 Sanchez, A. (2018). Emergent simplicity in microbial community assembly. *Science,*
1141 *361*(6401), 469-474.
1142 Goyal, A., Dubinkina, V., & Maslov, S. (2018). Multiple stable states in microbial communities
1143 explained by the stable marriage problem. *The ISME Journal*. doi:10.1038/s41396-018-
1144 0222-x
1145 Goyal, S., Yuan, J., Chen, T., Rabinowitz, J. D., & Wingreen, N. S. (2010). Achieving optimal
1146 growth through product feedback inhibition in metabolism. *PLoS computational biology,*
1147 *6*(6), e1000802.
1148 Hardin, G. (1960). The competitive exclusion principle. *Science, 131*(3409), 1292-1297.
1149 Huisman, J., Johansson, A. M., Folmer, E. O., & Weissing, F. J. (2001). Towards a solution of
1150 the plankton paradox: the importance of physiology and life history. *Ecology Letters,*
1151 *4*(5), 408-411.
1152 Huisman, J., van Oostveen, P., & Weissing, F. J. (1999). Species dynamics in phytoplankton
1153 blooms: incomplete mixing and competition for light. *The American Naturalist, 154*(1),
1154 46-68.
1155 Huisman, J., & Weissing, F. J. (1999). Biodiversity of plankton by species oscillations and
1156 chaos. *Nature, 402*(6760), 407-410. doi:10.1038/46540
1157 Huisman, J., & Weissing, F. J. (2001). Biological conditions for oscillations and chaos generated
1158 by multispecies competition. *Ecology, 82*(10), 2682-2695.
1159 Hutchinson, G. E. (1961). The paradox of the plankton. *The American Naturalist, 95*(882), 137-
1160 145.
1161 Kasting, J. F., & Siefert, J. L. (2002). Life and the evolution of Earth's atmosphere. *Science,*
1162 *296*(5570), 1066-1068. doi:10.1126/science.1071184
1163 Kerr, B., Riley, M. A., Feldman, M. W., & Bohannan, B. J. M. (2002). Local dispersal promotes
1164 biodiversity in a real-life game of rock–paper–scissors. *Nature, 418*(6894), 171.
1165 Koffel, T., Daufresne, T., Massol, F., & Klausmeier, C. A. (2016). Geometrical envelopes:
1166 Extending graphical contemporary niche theory to communities and eco-evolutionary
1167 dynamics. *Journal of Theoretical Biology, 407*, 271-289.
1168 Laland, K., Matthews, B., & Feldman, M. W. (2016). An introduction to niche construction
1169 theory. *Evol Ecol, 30*, 191-202. doi:10.1007/s10682-016-9821-z
1170 Leibold, M. A. (1995). The Niche Concept Revisited: Mechanistic Models and Community
1171 Context. *Ecology, 76*(5), 1371-1382. doi:10.2307/1938141
1172 Letten, A. D., Ke, P. J., & Fukami, T. (2017). Linking modern coexistence theory and
1173 contemporary niche theory. *Ecological Monographs, 87*(2), 161-177.
1174 doi:10.1002/ecm.1242
1175 Levin, S. A. (1970). Community equilibria and stability, and an extension of the competitive
1176 exclusion principle. *The American Naturalist, 104*(939), 413-423.

1177 Li, S. H.-J., Li, Z., Park, J. O., King, C. G., Rabinowitz, J. D., Wingreen, N. S., & Gitai, Z.
1178 (2018). Escherichia coli translation strategies differ across carbon, nitrogen and
1179 phosphorus limitation conditions. *Nature microbiology, 3*(8), 939.
1180 Liebermeister, W., Noor, E., Flamholz, A., Davidi, D., Bernhardt, J., & Milo, R. (2014). Visual
1181 account of protein investment in cellular functions. *Proceedings of the National Academy*
1182 *of Sciences, 111*(23), 8488-8493.
1183 Luli, G. W., & Strohl, W. R. (1990). Comparison of growth, acetate production, and acetate
1184 inhibition of Escherichia coli strains in batch and fed-batch fermentations. *Applied and*
1185 *environmental microbiology, 56*(4), 1004-1011.
1186 MacArthur, R. (1970). Species packing and competitive equilibrium for many species.
1187 *Theoretical Population Biology, 1*(1), 1-11.
1188 Maharjan, R., Seeto, S., Notley-McRobb, L., & Ferenci, T. (2006). Clonal adaptive radiation in a
1189 constant environment. *Science, 313*(5786), 514-517. doi:10.1126/science.1129865
1190 Marsland III, R., Cui, W., & Mehta, P. (2019). The Minimum Environmental Perturbation
1191 Principle: A New Perspective on Niche Theory. *arXiv preprint arXiv:1901.09673*.
1192 McGehee, R., & Armstrong, R. A. (1977). Some mathematical problems concerning the
1193 ecological principle of competitive exclusion. *Journal of Differential Equations, 23*(1),
1194 30-52.
1195 Moore, C., Mills, M., Arrigo, K., Berman-Frank, I., Bopp, L., Boyd, P., . . . Jaccard, S. (2013).
1196 Processes and patterns of oceanic nutrient limitation. *Nature Geoscience, 6*(9), 701.
1197 Murdoch, W. W., & Oaten, A. (1975). Predation and population stability.
1198 Mustonen, V., & Lässig, M. (2009). From fitness landscapes to seascapes: non-equilibrium
1199 dynamics of selection and adaptation. *Trends in Genetics, 25*(3), 111-119.
1200 doi:10.1016/j.tig.2009.01.002
1201 Odling-Smee, F. J., Laland, K. N., & Feldman, M. W. (2003). *Niche construction: the neglected*
1202 *process in evolution*: Princeton university press.
1203 Odum, E. P., & Barrett, G. W. (1971). *Fundamentals of ecology* (Vol. 3): Saunders Philadelphia.
1204 Palmer, M. W. (1994). Variation in species richness: Towards a unification of hypotheses. *Folia*
1205 *Geobotanica et Phytotaxonomica, 29*(4), 511-530. doi:10.1007/BF02883148
1206 Pfeiffer, T., & Bonhoeffer, S. (2004). Evolution of cross-feeding in microbial populations. *The*
1207 *American Naturalist, 163*(6), E126-E135.
1208 Posfai, A., Taillefumier, T., & Wingreen, N. S. (2017). Metabolic Trade-Offs Promote Diversity
1209 in a Model Ecosystem. *Physical Review Letters, 118*(2).
1210 doi:10.1103/PhysRevLett.118.028103
1211 Rosenzweig, R. F., Sharp, R., Treves, D. S., & Adams, J. (1994). Microbial evolution in a simple
1212 unstructured environment: genetic differentiation in Escherichia coli. *Genetics, 137*(4),
1213 903-917.
1214 Roy, S., & Chattopadhyay, J. (2007). Towards a resolution of 'the paradox of the plankton': A
1215 brief overview of the proposed mechanisms. *Ecological complexity, 4*(1-2), 26-33.
1216 Scheffer, M., Rinaldi, S., Huisman, J., & Weissing, F. J. (2003). Why plankton communities
1217 have no equilibrium: solutions to the paradox. *Hydrobiologia, 491*(1-3), 9-18.
1218 Schirrmeister, B. E., de Vos, J. M., Antonelli, A., & Bagheri, H. C. (2013). Evolution of
1219 multicellularity coincided with increased diversification of cyanobacteria and the Great
1220 Oxidation Event. *Proc Natl Acad Sci U S A, 110*(5), 1791-1796.
1221 doi:10.1073/pnas.1209927110

Smith, H. L., & Waltman, P. (1995). *The theory of the chemostat: dynamics of microbial competition* (Vol. 13): Cambridge university press.

Soliveres, S., Maestre, F. T., Ulrich, W., Manning, P., Boch, S., Bowker, M. A., . . . Allan, E. (2015). Intransitive competition is widespread in plant communities and maintains their species richness. *Ecology Letters, 18*(8), 790-798. doi:10.1111/ele.12456

Taillefumier, T., Posfai, A., Meir, Y., & Wingreen, N. S. (2017). Microbial consortia at steady supply. *eLife, 6*, e22644.

Tilman, D. (1980). Resources: a graphical-mechanistic approach to competition and predation. *The American Naturalist, 116*(3), 362-393.

Tilman, D. (1982). *Resource competition and community structure*: Princeton university press.

Tilman, D. (1994). Competition and Biodiversity in Spatially Structured Habitats. *Ecology, 75*(1), 2-16. doi:Doi 10.2307/1939377

Van den Bergh, B., Swings, T., Fauvart, M., & Michiels, J. (2018). Experimental design, population dynamics, and diversity in microbial experimental evolution. *Microbiol. Mol. Biol. Rev., 82*(3), e00008-00018.

Venturelli, O. S., Carr, A. C., Fisher, G., Hsu, R. H., Lau, R., Bowen, B. P., . . . Arkin, A. P. (2018). Deciphering microbial interactions in synthetic human gut microbiome communities. *Mol Syst Biol, 14*(6), e8157. doi:10.15252/msb.20178157

Wang, X., & Tang, C. (2017). Optimal growth of microbes on mixed carbon sources. *arXiv preprint arXiv:1703.08791*.

Wides, A., & Milo, R. (2018). Understanding the dynamics and optimizing the performance of chemostat selection experiments. *arXiv preprint arXiv:1806.00272*.

Wintermute, E. H., & Silver, P. A. (2010). Emergent cooperation in microbial metabolism. *Mol Syst Biol, 6*, 407. doi:10.1038/msb.2010.66

Wright, S. (1932). *The roles of mutation, inbreeding, crossbreeding, and selection in evolution* (Vol. 1): na.

Zhang, X. S. (2012). Fisher's geometrical model of fitness landscape and variance in fitness within a changing environment. *Evolution: International Journal of Organic Evolution, 66*(8), 2350-2368.

Ziv, N., Brandt, N. J., & Gresham, D. (2013). The Use of Chemostats in Microbial Systems Biology. *Jove-Journal of Visualized Experiments*(80). doi:UNSP e50168 10.3791/50168

FIGURES

Figure 1

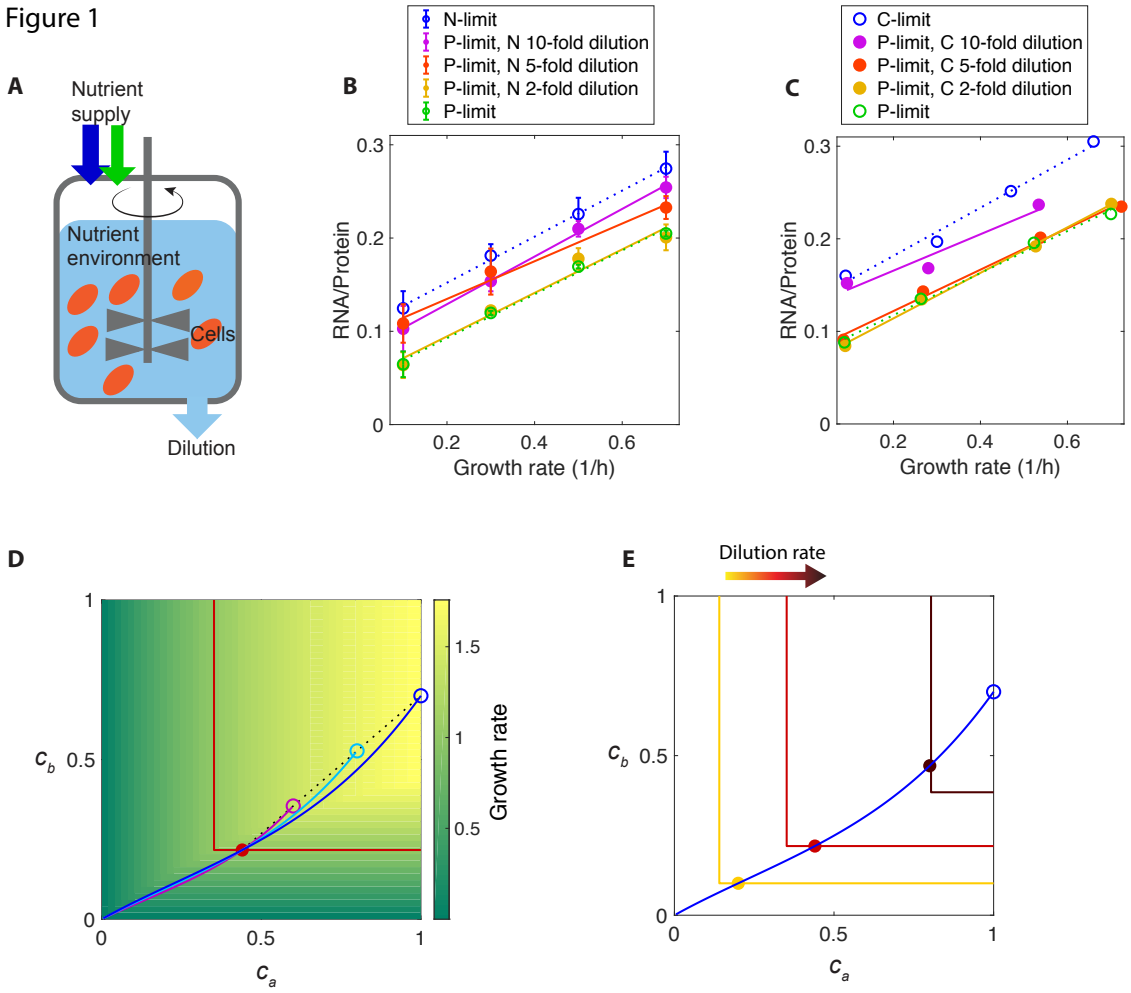

Figure 1 - Chemostat behavior can be represented in the space of nutrient concentrations.

A. Schematic diagram of a chemostat occupied by a single microbial species. In the well-mixed medium (pale blue) of a chemostat, cells (orange ellipses) consume nutrients and grow. An influx of nutrients with fixed concentrations (blue and green arrows) is supplied at the same rate as dilution, keeping the medium volume constant.

B. Nutrient supply shifts the relationship between RNA/Protein ratio and growth rate of *E. coli* cultured in chemostats from phosphorus limitation (P-limited, green open circles and dotted line) to nitrogen limitation (N-limited, blue open circles and dotted line). Data for dilution of supplied nitrogen by 2, 5, and 10-fold starting from the P-limited condition are shown as solid dots and corresponding best-fit lines. Each measurement was repeated three times and standard errors are shown by bars.

C. Same as (B), but for phosphorus and carbon limitation instead of phosphorus and nitrogen limitation. Data for dilution of supplied carbon by 2, 5, and 10-fold starting from the P-limited condition are shown as solid dots and corresponding best-fit lines.

D. Visual representation of how a species creates its own chemostat environment. Background color indicates the growth rate of cells as a function of nutrient concentrations c_a and c_b, with the growth contour shown by the red curve. The supply line for the steady-state environment (purple dot) is shown as a dotted black line. Different supply concentrations ($c_{a,\mathrm{supply}}$ and $c_{b,\mathrm{supply}}$) along the supply line are marked by purple, cyan, and blue circles, with the corresponding flux-balance curves shown in the same colors.

E. Dilution rate can flip nutrient limitation. The external supply condition is marked by a blue circle, and the flux-balance curve for this supply is shown in the same color. Three growth contours with increasing dilution rates are shown from yellow to deep red, and the corresponding steady-state environments are shown in colored dots.

Figure 2

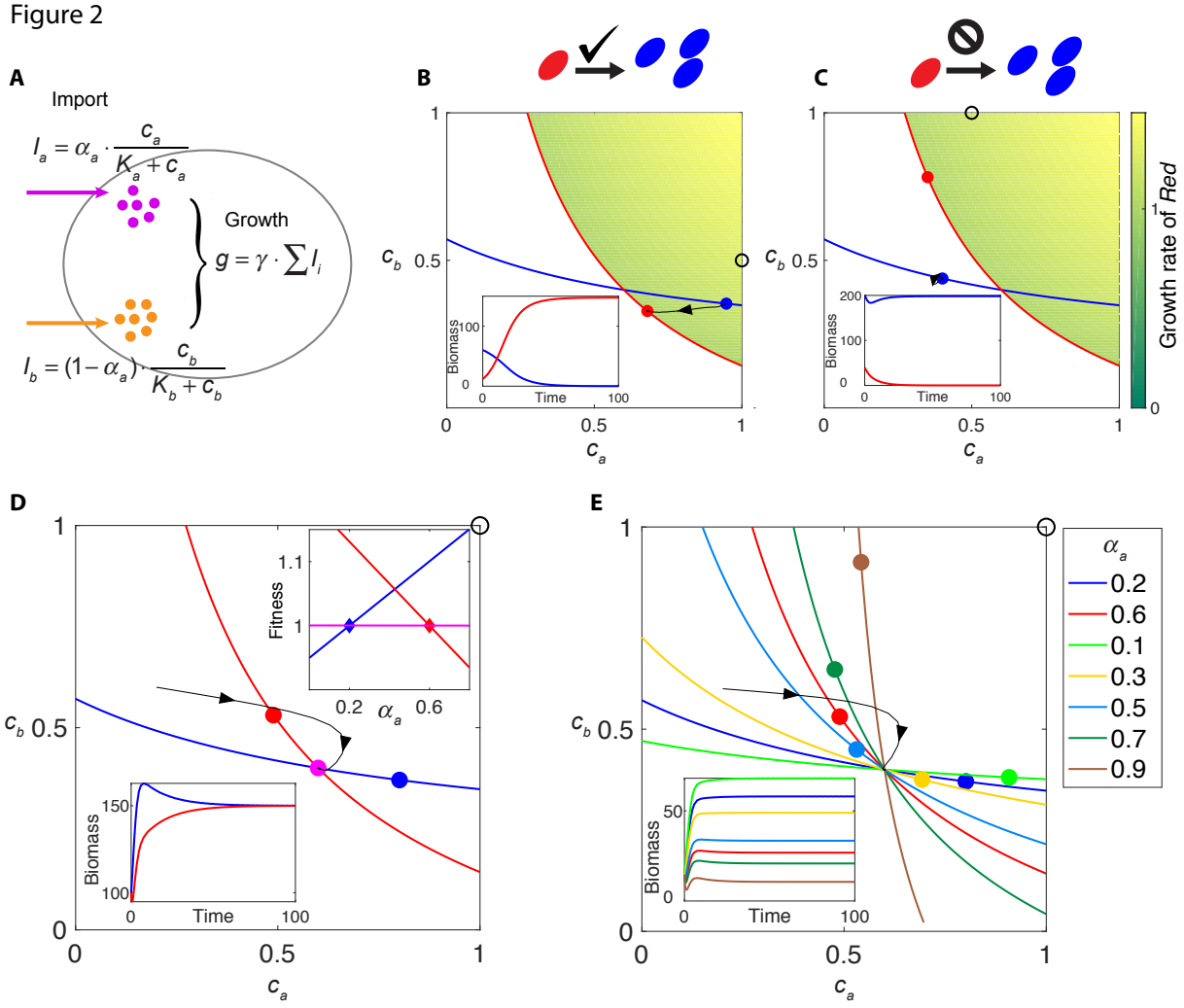

Figure 2 – Invasion and coexistence in a chemostat.

A. Example of a metabolic model with a trade-off in allocation of resources for import of two substitutable nutrients, with both nutrients contributing additively to growth. Species *Red* and species *Blue* allocate resources differently (indicated by parameter α_a, see Methods).

B. Example of successful invasion of species *Blue* by species *Red*. A small amount of species *Red* is introduced to a steady-state chemostat of species *Blue*. Growth contours and steady-state environments of species *Blue* and species *Red* are shown as curves and dots in the corresponding colors (colored background indicates the “invasion zone” of *Red*, and represents the growth rate of *Red* in this zone). The supply condition is marked by black circle. Black curves with arrows show the time trajectory of the invasion in nutrient space. Inset: biomass of species in chemostat over time course of invasion.

C. Same as (B), except that because the supply condition (black circle) is different, the attempted invasion by species *Red* is unsuccessful.

D. Growth contours and the steady-state environments created by *Red* or *Blue* alone, under the supply condition shown by the black circle. Black curve with arrows shows a trajectory in nutrient space. Purple dot indicates the steady-state environment created by *Red* and *Blue* together. Lower inset: time course of species biomass. Upper inset: the fitness landscape created by *Red* alone (color red, with the strategy of *Red* marked by red diamond), created by *Blue* alone (color blue, with the strategy of *Blue* marked by blue diamond), and created by both species (color purple). The colors correspond to the steady-state environments shown by colored dots in (D).

E. Growth contours and the species-specific steady-state environments for seven different species alone, under the supply condition shown by the black circle. Black curve with arrows shows a trajectory in nutrient space. Lower inset: time course of species biomass.

Figure 3

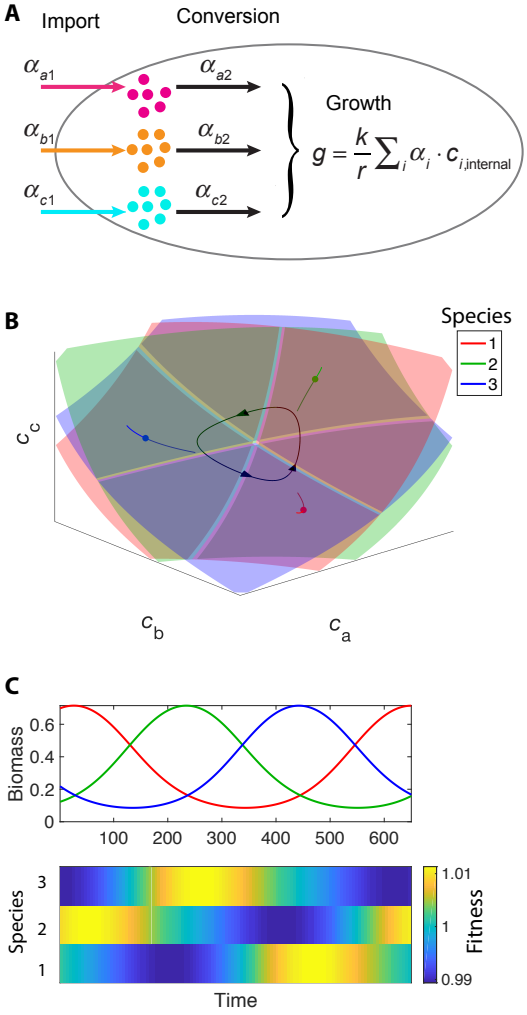

Figure 3 - Rock-paper-scissors oscillations.

A. Example of a metabolic model with a trade-off in allocation of resources for importing of three substitutable nutrients and assimilating them into biomass, with all three nutrients contributing additively to growth. Species *Red*, species *Blue*, and species *Green* allocate resources differently (see Methods).

B. Growth contours (surfaces), flux-balance curves (lines), and steady-state nutrient concentrations (dots) for the three species in a three-dimensional nutrient space. Black curves with arrows show the system's limit-cycle trajectory.

C. The top panel shows the time course of species biomass for the limit cycle in (B). The bottom panel shows how the fitness landscape changes with time over one period of the oscillation.

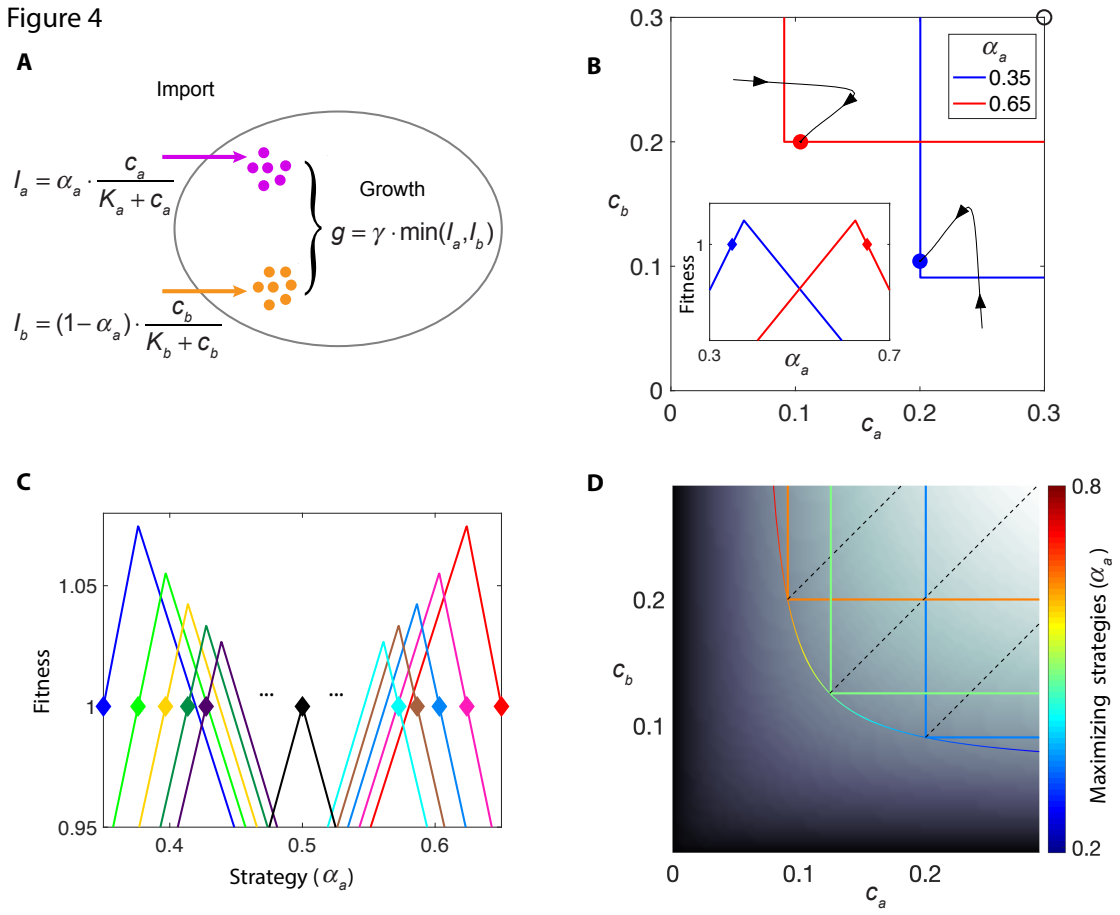

Figure 4 – Multi-stability, chain of invasion, and non-invasible strategy.

A. Example of bistability for a metabolic model with a trade-off in allocation of resources for import of two essential nutrients, with the lower of the two import rates determining growth rate. Species *Red* and species *Blue* allocate resources differently (indicated by parameter α_a, see Methods).

B. Bistability of the system in (A) shown in nutrient space. Black curves with arrows show the trajectories of simulations with different initial conditions. Inset: the fitness landscape created by species *Red* or *Blue* alone, with colors corresponding to the steady-state environments shown by colored dots in (B).

C. A chain of invasion. Fitness landscape created by species with different resource allocation strategies (marked by diamond shapes). Starting from species *Blue*, the species having the highest growth rate in the fitness landscape created by the "former" species is chosen. This creates a chain of invasion from *Blue* to *Light Green*, *Yellow*, *Deep Green*, *Deep Purple*, all the way (intermediate processes omitted) to the species *Black*, which places itself on the peak of its fitness landscape. The same procedure is also performed starting with species *Red*.

D. Depiction of non-invasible strategies under different supply conditions. Black-white background indicates the maximal growth rate of model in (A) under each environment, and the contour of maximal growth rates contains different strategies (represented by red-to-blue color). Growth contours of three species adopting one of the “maximizing strategies” are colored by their strategies. The supply conditions allowing these strategies to be “non-invasible” are marked by dashed black lines.

Figure 5

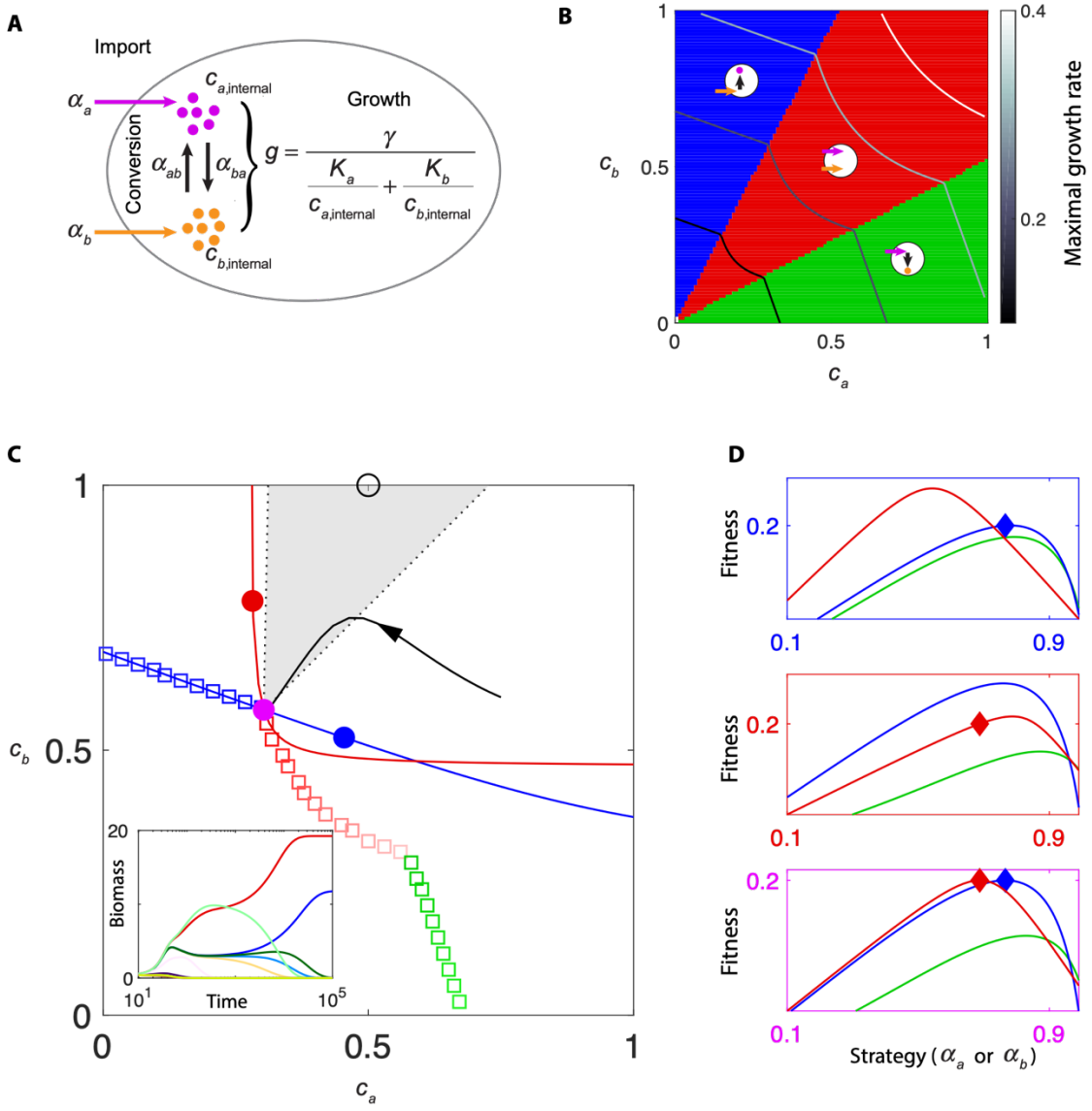

Figure 5 - Non-invasible cartels.

A. Metabolic model with a trade-off in allocation of resources for import of two nutrients plus their interconversion, with both nutrients necessary for growth.

B. Three subclasses of maximizing metabolic strategies in nutrient space are indicated by background color, and circles with arrows illustrate the metabolic strategies of each subclass. The maximal growth contours for four growth rates (0.1, 0.2, 0.3, 0.4) are marked by gray colors.

C. Two maximizing strategies co-creating a non-invasible steady state. At dilution rate 0.2, the maximal growth contour and the corresponding maximizing strategies are shown as colored squares. At a discontinuous point of the growth contour, the supply

lines of two distinct metabolic strategies (*Red* and *Blue*) span a gray region, where any supply condition (e.g. black circle) requires the two maximizing strategies to co-create the environment on the discontinuous point. Red and blue dots mark the environments created by species *Red* and species *Blue* alone, and the purple dot marks the environment co-created by *Red* and *Blue*. Black curve with arrows shows a trajectory in nutrient space. Inset is the competition dynamics of the species *Red* and species *Blue* together with 10 other maximizing species with different strategies.

D. The fitness landscapes for the three environments in (C) indicated by corresponding box colors. For class Green and Red, the strategy is represented by α_a, for class Blue, the strategy is represented by α_b.

Figure 6

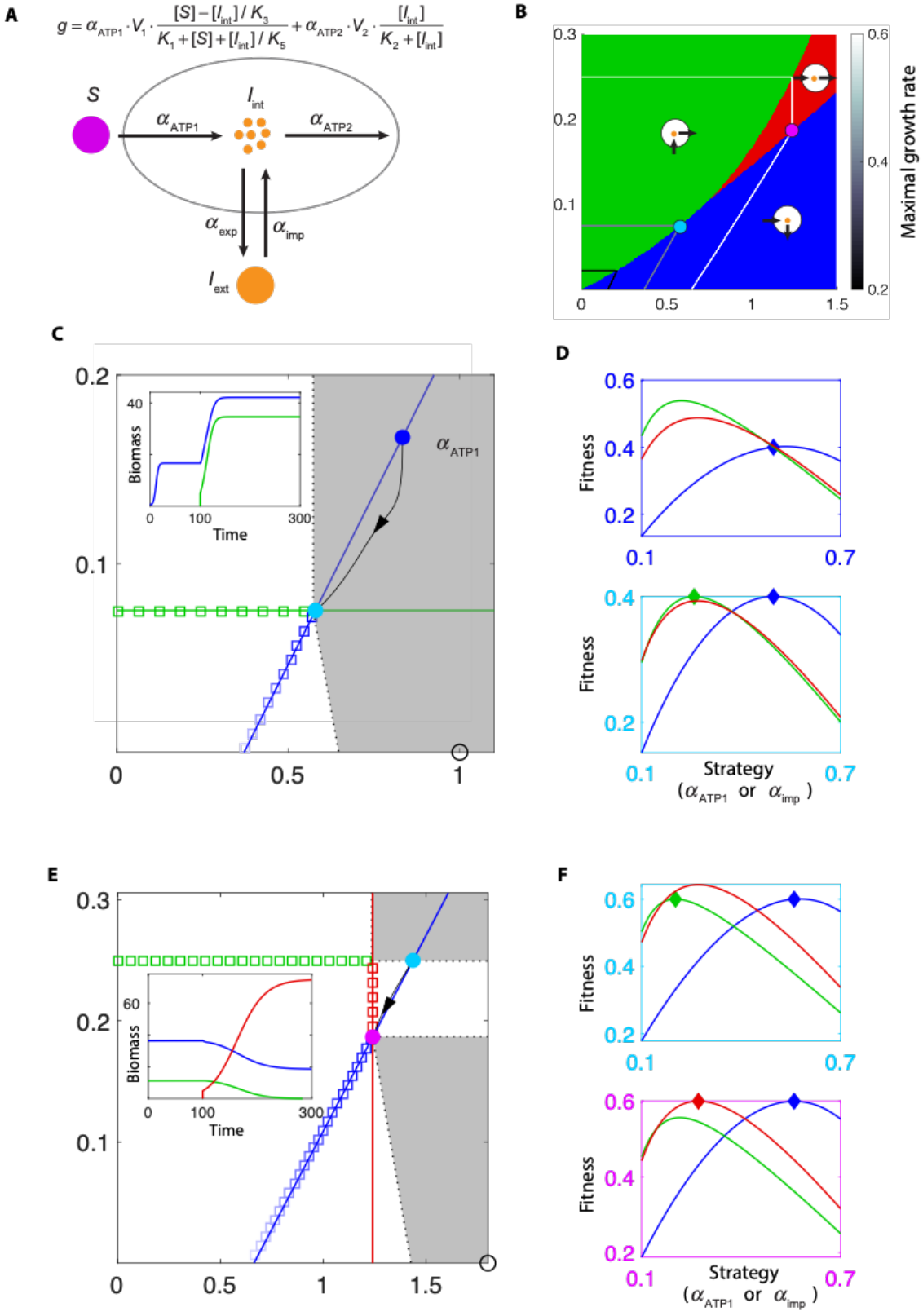

Figure 6 – Species creating new nutrient dimensions and achieving evolutionarily stable coexistence.

A. Metabolic model with a single supplied nutrient *S*. Cells allocate enzymes to convert *S* into internal intermediate I_{int} and produce energy (denoted as "ATP"), export internal intermediate into the chemostat to become I_{ext}, import external intermediate, or consume I_{int} to produce ATP. The growth rate is the sum of ATP production (see Methods).

B. Three subclasses of maximizing metabolic strategies in nutrient space are indicated by background color, and circles with arrows illustrate the metabolic strategies of each subclass. The maximal growth contours for three growth rates (0.2, 0.4, 0.6) are marked by black-to-white colors.

C. At dilution rate 0.4, two maximizing strategies co-create a non-invasible environment. The maximal growth contour and the corresponding maximizing strategies are shown as colored squares. At a discontinuous point of the growth contour, the supply lines of two distinct metabolic strategies (*Green* and *Blue*) span a gray region, where any supply condition (e.g. black circle) requires two maximizing strategies to co-create the environment at the discontinuous point. Blue dot marks the environment created by species *Blue* alone, and the cyan dot marks the environment co-created by *Blue* and *Green*. Black curve with arrows shows a trajectory in nutrient space. Inset shows the time course of species biomass, with species *Green* added to the chemostat at time 100.

D. The fitness landscapes for two environments in (C) indicated by corresponding box colors, reflecting the relationship between instantaneous growth rate and resource allocation strategy. For class Blue and Red, the strategy is represented by α_{ATP1}; for class Green the strategy is represented by α_{imp}.

E. Same as (C), except that the dilution rate is 0.6, and the inset shows the time course of species biomass, starting with *Blue* and *Green*, with species *Red* added to the chemostat at time 100.

D. Same as (D), except that it is for the two steady-state environments shown in (E).

SUPPLEMENTAL FIGURES

Figure S1

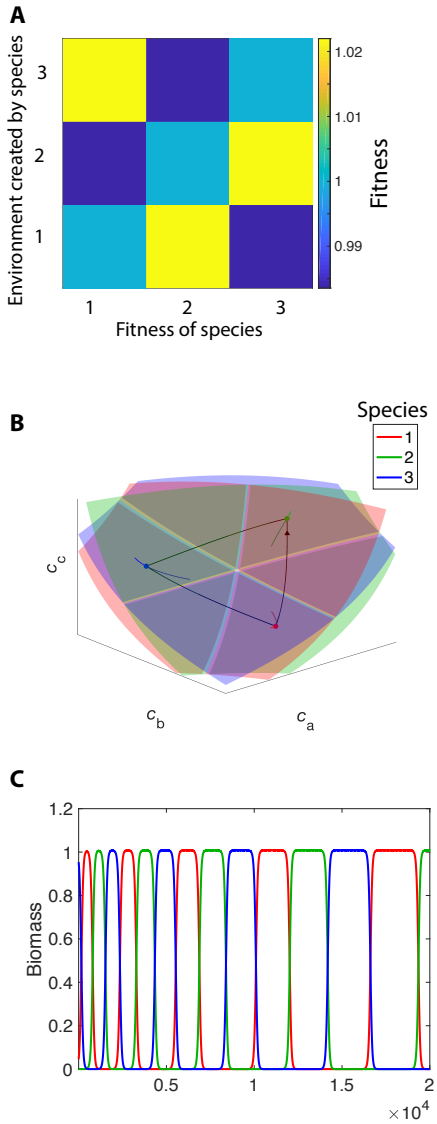

Figure S1- Rock-paper-scissor fitness landscape and heteroclinic cycle

A. The fitness of Species 1, 2, and 3 in the steady-state environment constructed by species 1, 2, and 3 for the model in Fig 3.

B. Growth contours (surfaces), flux-balance curves (lines), and steady-state nutrient concentrations (dots) for three species in a three-dimensional nutrient space, with a different conversion speed ($k = 10$) than in Fig. 3 ($k = 1$) (see Methods). Black curves with arrows show the system's oscillatory trajectory.

C. The top panel shows the time course of species biomass for the limit cycle in (B). The bottom panel shows how the fitness landscape changes with time.

D. Time course of species biomass over a long duration.

Figure S2

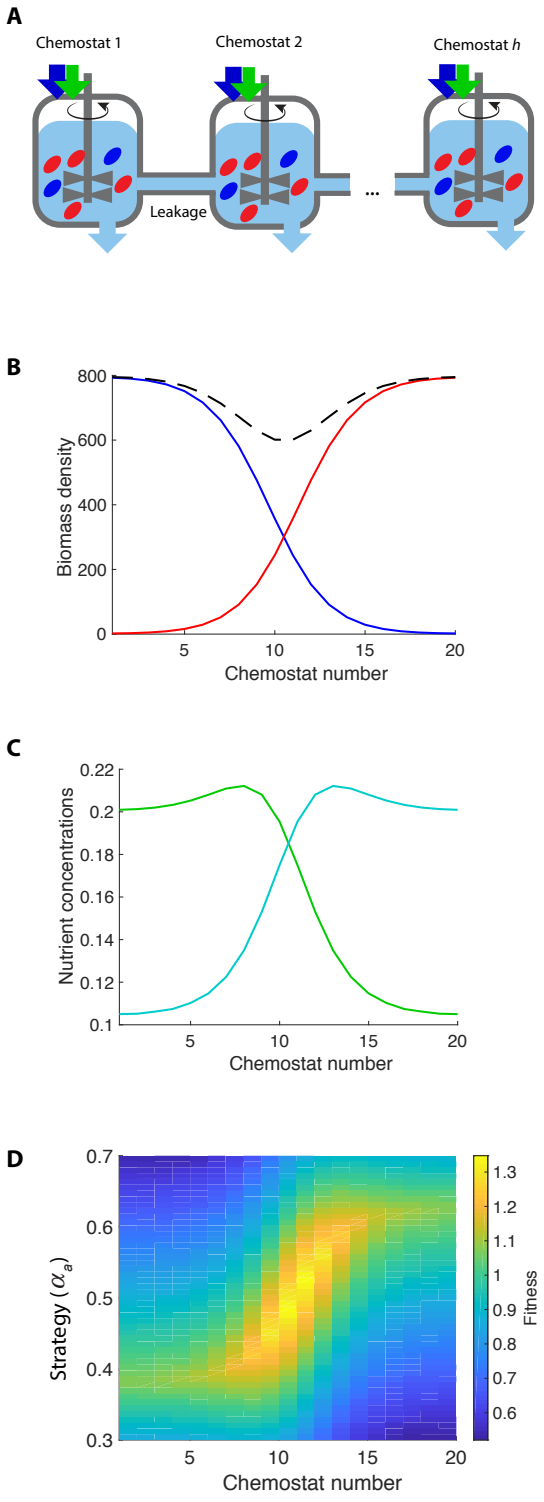

Figure S2- Steady-state spatial heterogeneity for linked chemostats.

With initial seeding of two species, one at each of the two ends of a chain of chemostats, a steady-state gradient of species biomass density spontaneously emerges accompanied by a gradient of nutrient concentrations, even though the supply conditions and dilution rates are identical for all the chemostats.

A. Schematic of k_{tot} linked chemostats exchanging medium and cells via leakage, described by Eqs. S34-S35. The two species in the chemostats (*Blue* and *Red*) are the same bistable pair as in Fig 4B and the leakage rate is $l = 1$.

B. The species composition along 20 linked chemostats for the system in (A). Species colors correspond to those in Fig 4B, with species *Blue* having $\alpha_a = 0.35$, species *Red* having $\alpha_a = 0.65$. The dashed black curve shows the sum of the two biomass densities. The initial condition was cell-free chemostats with a small amount of *Blue* added to Chemostat 1 and small amount of *Red* added to Chemostat 20.

C. Concentrations along the 20 chemostats for nutrient *a* (green) and nutrient *b* (cyan) for system in (A).

D. The fitness landscape along the chain of chemostats. The *x*-axis is the 20 linked chemostats, and the *y*-axis is the metabolic strategy represented by α_a. Color indicates the growth rate of species adopting the given strategy in the *k*-th chemostat.

Figure S3

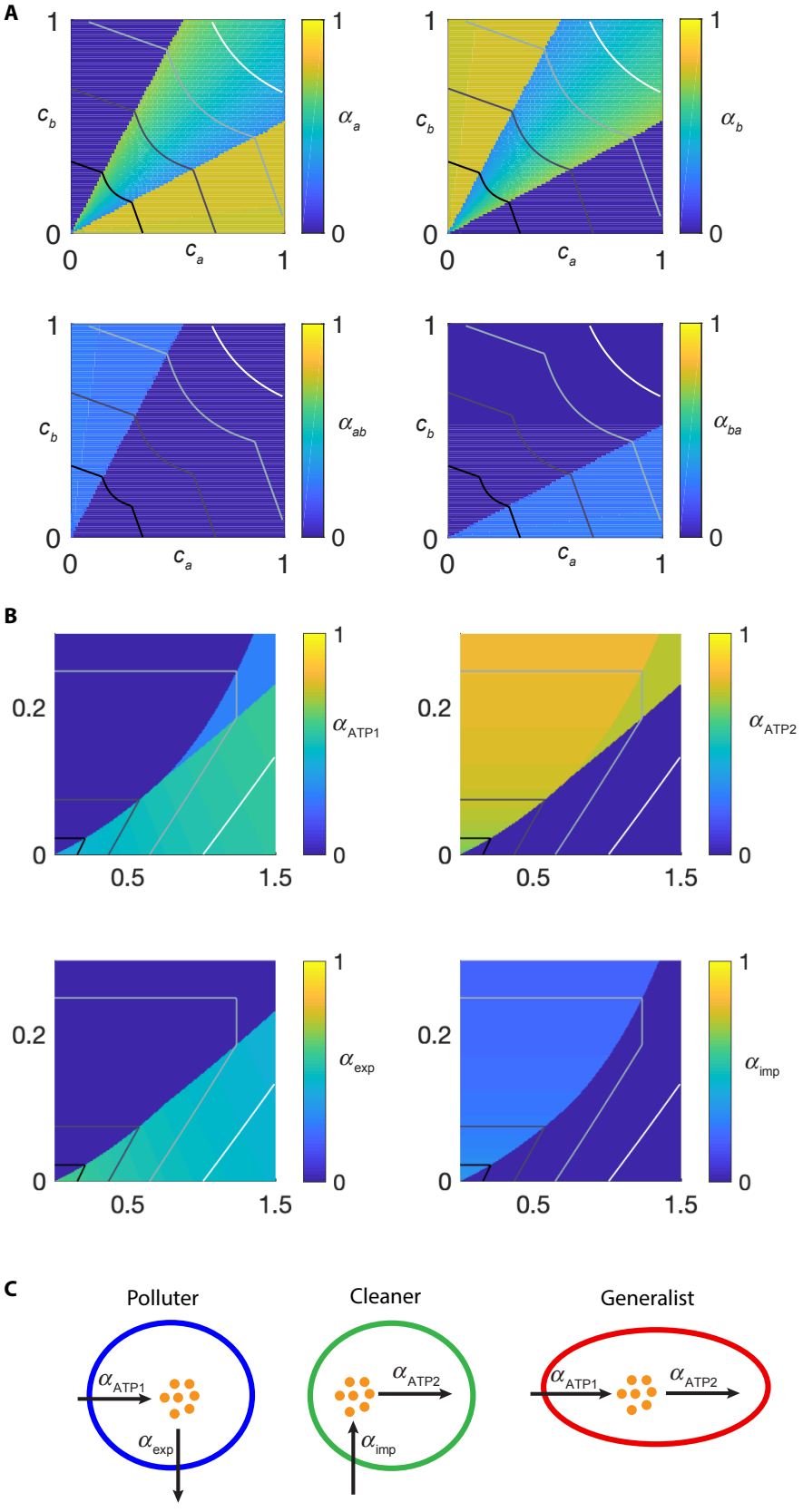

Figure S3 – Maximizing strategies in nutrient space.

A. For each environment in the nutrient space, the maximizing resource allocation strategies that maximizes growth rates for the model in Fig 5A. Each strategy is represented by the four elements [α_a, α_b, α_{ab}, α_{ba}], and values for each element are shown by a heatmap. Black-to-white curves are the maximal growth contours for $d = 0.1, 0.2, 0.3, 0.4$.

B. For each environment in the nutrient space, the maximizing resource allocation strategies that maximizes growth rates for the model in Fig 6A. Each strategy is represented by the four elements [α_{ATP1}, α_{ATP2}, α_{exp}, α_{imp}], and values for each element are shown by a heatmap. Black-to-white curves are the maximal growth contours for $d = 0.2, 0.4, 0.6$.

C. Schematic representations of the three classes of maximizing strategies appearing in (B).